Monthly Notices
of the
ROYAL ASTRONOMICAL SOCIETY

MNRAS **435,** 2806–2821 (2013) doi:10.1093/mnras/stt1430
Advance Access publication 2013 September 20

Hierarchical clustering in chameleon *f*(*R*) gravity

Wojciech A. Hellwing,[1,2]⋆ Baojiu Li,[1]⋆ Carlos S. Frenk[1] and Shaun Cole[1]

[1]*Institute for Computational Cosmology, Department of Physics, Durham University, South Road, Durham DH1 3LE, UK*
[2]*Interdisciplinary Centre for Mathematical and Computational Modelling (ICM), Univesity of Warsaw, ul. Pawińskiego 5a, 02-106 Warsaw, Poland*

Accepted 2013 July 30. Received 2013 July 29; in original form 2013 May 31

ABSTRACT

We use a suite of high-resolution state-of-the-art *N*-body dark matter simulations of chameleon *f*(*R*) gravity to study the higher order volume-averaged correlation functions $\overline{\xi_n}$ together with the hierarchical *n*th-order correlation amplitudes $S_n = \overline{\xi}_n/\overline{\xi}_2^{n-1}$ and density distribution functions (PDF). We show that under the non-linear modifications of gravity the hierarchical scaling of the reduced cumulants is preserved. This is however characterized by significant changes in the values of both $\overline{\xi_n}$ and S_n and their scale dependence with respect to General Relativity gravity (GR). In addition, we measure a significant increase of the non-linear σ_8 parameter reaching 14, 5 and 0.5 per cent in excess of the GR value for the three flavours of our *f*(*R*) models. We further note that the values of the reduced cumulants up to order $n = 9$ are significantly increased in *f*(*R*) gravity for all our models at small scales $R \lesssim 30\,h^{-1}$ Mpc. In contrast, the values of the hierarchical amplitudes, S_n, are smaller in *f*(*R*) indicating that the modified gravity density distribution functions are deviating from the GR case. Furthermore, we find that the redshift evolution of relative deviations of the *f*(*R*) hierarchical correlation amplitudes is fastest at high and moderate redshifts $1 \leq z \leq 4$. The growth of these deviations significantly slows down in the low-redshift universe. We also compute the PDFs and show that for scales below $\sim 20\,h^{-1}$ Mpc, they are significantly shifted in *f*(*R*) gravity towards the low densities. Finally, we discuss the implications of our theoretical predictions for measurements of the hierarchical clustering in galaxy redshift surveys, including the important problems of the galaxy biasing and redshift space distortions.

Key words: gravitation – cosmology: theory – dark energy – dark matter – large-scale structure of Universe.

1 INTRODUCTION

The parameters of the standard model of cosmology – *the Lambda cold dark matter model* – based on the Einstein theory of *General Relativity* (hereafter LCDM and GR, respectively) have been established to an outstanding precision (e.g. Cole et al. 2005; Eisenstein et al. 2005; Hinshaw et al. 2012; Planck Collaboration 2013). The growing observational evidence has somehow not been fully matched by an appropriate development of theoretical understanding. Unfortunately, we are still left with the riddles and puzzles of dark matter (DM) and dark energy. While there is not much doubt in the existence of the former, the latter part of the model which is supposed to account for the observed accelerated expansion of the Universe (Riess et al. 1998; Perlmutter et al. 1999) has an elusive and not fully understandable physical nature. The accelerated expansion of the Universe is usually accounted for by either assuming an extremely low value of the Einstein cosmological constant Λ, or by postulating its value to be zero and invoking the background scalar field to drive the accelerated expansion (e.g. Peebles & Ratra 1988; Ratra & Peebles 1988; Zlatev, Wang & Steinhardt 1999; Amendola 2000; Kamenshchik, Moschella & Pasquier 2001). Both approaches however suffer from the well-known coincidence and fine tuning problems (see, e.g. Carroll 2001, and references therein). However, it is also possible to obtain an accelerated universe by modifying the GR equations that govern the background evolution of the Universe (e.g. Carroll et al. 2004), i.e. by implementing a modified gravity model. Such modifications can be done in many ways. In recent years, one of the possible modifications that gained much attention consists of the class of models called the *f*(*R*) gravity. Here, the Einstein–Hilbert action is augmented with an arbitrary, intrinsically non-linear function *f* whose argument is the Ricci or curvature scalar *R* (e.g. Carroll et al. 2005; de Felice & Tsujikawa 2010; Sotiriou & Faraoni 2010; Nojiri & Odintsov 2011). The *f*(*R*) gravity models are very interesting as they have potentially rich physics. Not only can modified action fuel the accelerated expansion but also due to the propagation of an extra scalar degree of freedom can give rise to a fifth-force or Newtonian gravity enhancement (Chiba 2003; Chiba, Smith & Erickcek 2007). This in turn can have potentially interesting effects on galaxy and large-scale structure formation and

⋆E-mail: pchela@icm.edu.pl (WAH); baojiu.li@durham.ac.uk (BL)

matter clustering patterns. Albeit we ought to stress out that also the $f(R)$ gravity theories need a significant amount of fine tuning of their parameters to allow for a viable universe (e.g. Hu & Sawicki 2007; Erickcek et al. 2013).

If $f(R)$ gravity is to be a feasible theory describing the observable Universe, it must pass local gravity tests. Hence, the fifth-force it introduces must be suppressed in high-density regions, like our Solar system. This is achieved by the appropriate choice of the $f(R)$ function that leads to the so-called *chameleon mechanism*. This non-linear process traps the scalar field in high-density (high-curvature) regions and constrains the local deviations from the usual GR gravity. The intrinsic non-linear character of the chameleon mechanism makes all predictions for clustering statistics in an $f(R)$ universe very difficult. As the degree of non-linearity grows both in the matter density and scalar fields, perturbation theory predictions quickly become inaccurate (e.g. Li et al. 2013). Hence, study of the cosmological implications of a chameleon $f(R)$ gravity calls for a use of the high-resolution N-body simulations. We base studies presented in this paper on a recently performed suite of high-resolution state-of-the-art chameleon $f(R)$ N-body simulations conducted with a use of the novel code – the ECOSMOG (Li et al. 2012a).

The standard model of the formation of large-scale structure is based on two conventional assumptions. The first is that structures grew from an initially tiny Gaussian density fluctuation. The second belongs to the mechanism responsible for growth of perturbations, which is taken to be gravitational instability. This, supplemented by the cold nature of the main matter ingredient (the DM), leads to a hierarchical model of structure formation, where the clustering proceeds from small to large scales. For power-law spectra, $P \propto k^{n_s}$, this is always true, provided $n_s > -3$. In the $f(R)$ gravity, all ingredients of the structure formation model are the same as in the standard one, except for the non-linear modifications to local gravity – the fifth-force, which must lead to non-trivial modifications of the growth mechanism.

All tests of theories for the origin of the large-scale structure of the universe, including the modified gravity, rely on a comparison of model predictions with measurable quantities, derived from observations. The statistical measures we will discuss in this paper are the low- and high-order volume-averaged n-point correlation functions (or connected moments) $\overline{\xi}_n$ of the density field. These estimators have two clear advantages. First, they can be related to the underlying DM dynamics (Peebles 1980; Juszkiewicz, Bouchet & Colombi 1993; Gaztanaga & Baugh 1995; Juszkiewicz & Bouchet 1995). Secondly, they can be measured and extracted from galaxy surveys (see e.g. Gaztanaga 1994; Zaldarriaga, Seljak & Hui 2001; Baugh et al. 2004; Croton et al. 2004; Gaztañaga et al. 2005; Ross, Brunner & Myers 2007, and the references therein) and N-body simulations (e.g. Bouchet & Hernquist 1992; Baugh, Gaztanaga & Efstathiou 1995; Szapudi & Colombi 1996; Szapudi et al. 1999; Angulo, Baugh & Lacey 2008; Hellwing, Juszkiewicz & van de Weygaert 2010), with a reasonable degree of fidelity and reproducibility.

The set of n-point connected moments constitute a simple, yet elegant and complete description of the statistical properties of the cosmic density field. One of the fundamental predictions of the classical gravitational instability model is that the gravitational evolution of the initially Gaussian density field in an expanding universe generates higher order correlations, $\overline{\xi}_n$ with $n > 2$, which exhibit so-called *hierarchical scaling*. That is, the higher order moments scale with variance as $\overline{\xi}_n = S_n \overline{\xi}_2^{n-1}$. The S_n numbers are called *hierarchical amplitudes* and are weakly monotonic functions of scale R. The hierarchical amplitudes only very weakly depend on Ω_M and Ω_Λ (the matter and dark energy cosmic densities). Moreover, galaxy biasing and redshift space distortions do not break down the hierarchical scaling of the higher order moments. This behaviour of higher order clustering statistics was largely confirmed for the standard GR model using both theoretical (Fry 1984a,b; Fry & Gaztanaga 1993, 1994; Bouchet et al. 1995; Hivon et al. 1995) and observational evidence (Gaztanaga 1994; Baugh et al. 2004; Croton et al. 2004; Gaztañaga et al. 2005; Ross et al. 2007).

Because the hierarchical scaling and clustering was so thoughtfully tested for standard GR model paradigm, it is crucial to establish predictions for the correlation hierarchy in the $f(R)$ and any other realistic modified gravity model. This is the main goal and aim of this paper. The high-order correlations hierarchy was studied for a simple model of a fifth-force modified gravity by Hellwing et al. (2010). They found that even in the regime of modified dynamics, the hierarchical scaling is preserved, although the values of S_n and their scale and time dependence deviate from the standard model. Their model however assumed very simple phenomenological form of modified gravity. In this work, we study for the first time the high-order correlations for a more physically motivated $f(R)$ gravity model with a full treatment of the non-linear chameleon mechanism.

2 THE $f(R)$ GRAVITY THEORY

This section is devoted to a brief review of the $f(R)$ gravity theory and its theoretical properties.

2.1 The $f(R)$ gravity model

The $f(R)$ gravity model (Carroll et al. 2005) is a generalization of GR achieved by replacing the Ricci scalar R in the Einstein–Hilbert action with an algebraic function $f(R)$ (see e.g. de Felice & Tsujikawa 2010; Sotiriou & Faraoni 2010, for most recent reviews):

$$S = \int \mathrm{d}^4x\sqrt{-g}\left\{\frac{M_{\rm Pl}^2}{2}\left[R + f(R)\right] + \mathcal{L}_{\rm m}\right\}, \tag{1}$$

in which $M_{\rm Pl}$ is the reduced Planck mass, $M_{\rm Pl}^{-2} = 8\pi G$, G is Newton's constant, g the determinant of the metric $g_{\mu\nu}$ and $\mathcal{L}_{\rm m}$ the Lagrangian density for matter and radiation fields (including photons, neutrinos, baryons and CDM). By designing the functional form of $f(R)$, one can fully specify an $f(R)$ gravity model.

Varying the action, equation (1), with respect to the metric field $g_{\mu\nu}$, one obtains the modified Einstein equation

$$G_{\mu\nu} + f_R R_{\mu\nu} - g_{\mu\nu}\left[\frac{1}{2}f - \Box f_R\right] - \nabla_\mu\nabla_\nu f_R = 8\pi G T^m_{\mu\nu}, \tag{2}$$

where $G_{\mu\nu} \equiv R_{\mu\nu} - \frac{1}{2}g_{\mu\nu}R$ is the Einstein tensor, $f_R \equiv \mathrm{d}f/\mathrm{d}R$, ∇_μ is the covariant derivative compatible with $g_{\mu\nu}$, $\Box \equiv \nabla^\alpha\nabla_\alpha$ and $T^m_{\mu\nu}$ is the energy momentum tensor of matter and radiation fields. Equation (2) is a fourth-order differential equation, but can also be considered as the standard second-order equation of GR with a new dynamical degree of freedom, f_R, the equation of motion of which can be obtained by taking the trace of equation (2)

$$\Box f_R = \frac{1}{3}\left(R - f_R R + 2f + 8\pi G\rho_{\rm m}\right), \tag{3}$$

where $\rho_{\rm m}$ is the matter density. The new degree of freedom f_R is often dubbed *the scalaron* in the literature (e.g. Zhao, Li & Koyama 2011).

If the background Universe is described by the flat Friedmann–Robertson–Walker (FRW) metric, the line element of the real, perturbed, Universe can be written in the conformal Newtonian gauge

as

$$ds^2 = a^2(\eta)\left[(1+2\Phi)d\eta^2 - (1-2\Psi)dx^i dx_i\right], \quad (4)$$

where η and x^i are the conformal time and comoving coordinates, $\Phi(\eta, \boldsymbol{x})$ and $\Psi(\eta, \boldsymbol{x})$ are, respectively, the Newtonian potential and perturbed spatial curvature, which are functions of both time η and space $\boldsymbol{x}$; a denotes the scale factor of the Universe with a normalization of $a = 1$ today.

We will be mainly interested in large-scale structure on scales much smaller than the Hubble scale. Since the time variation of f_R is very small in the models to be considered below, we shall work in the quasi-static limit by neglecting the time derivatives of f_R. Under this limit, the f_R equation of motion – equation (3), reduces to

$$\vec{\nabla}^2 f_R = -\frac{1}{3}a^2\left[R(f_R) - \bar{R} + 8\pi G\left(\rho_{\rm m} - \bar{\rho}_{\rm m}\right)\right], \quad (5)$$

where $\vec{\nabla}$ is the three-dimensional gradient operator (an arrow is used to distinguish this from the ∇ introduced above), and the overbar takes the background average of a quantity. Note that R can be expressed as a function of f_R by reverting $f_R(R)$.

Similarly, the Poisson equation, which governs the behaviour of the Newtonian potential Φ, simplifies to

$$\vec{\nabla}^2\Phi = \frac{16\pi G}{3}a^2\left(\rho_{\rm m} - \bar{\rho}_{\rm m}\right) + \frac{1}{6}a^2\left[R\left(f_R\right) - \bar{R}\right], \quad (6)$$

by neglecting terms involving time derivatives of Φ and f_R, and using equation (5) to eliminate $\vec{\nabla}^2 f_R$.

The above equations imply two potential cosmological effects of the scalaron field: (i) the background expansion of the Universe can be modified by the new terms in equation (2) and (ii) the relationship between the gravitational potential Φ and the matter density field is modified, which can cause changes in the matter clustering and growth of density perturbations. Evidently, when $|f_R| \ll 1$, we have $R \approx -8\pi G\rho_{\rm m}$ according to equation (5) and so equation (6) reduces to the normal Poisson equation of GR; when $|f_R|$ is large, we instead have $|R - \bar{R}| \ll 8\pi G|\rho_{\rm m} - \bar{\rho}_{\rm m}|$ and then equation (6) reduces to the normal Poisson equation with G rescaled by 4/3. The value 1/3 is the maximum enhancement factor of gravity in $f(R)$ models, independent of the specific functional form of $f(R)$. The choice of $f(R)$, however, is important because it determines the scalaron dynamics and therefore when and on which scale the enhancement factor changes from 1 to 4/3: scales much larger than the range of the modification to Newtonian gravity mediated by the scalaron field (i.e., the Compton wavelength of f_R) are unaffected and gravity is not enhanced there, while on small scales, depending on the environmental matter density, the 1/3 enhancement may be fully realized – this results in a scale-dependent modification of gravity and therefore a scale-dependent growth rate of structures.

2.2 The chameleon mechanism

The local test of gravity, based on the Solar system observations, provides tight constraints on any deviations from a Newtonian gravity (Hu & Sawicki 2007; Berry & Gair 2011). The classical $f(R)$ model is then strongly ruled out due to its factor-of-4/3 enhancement to the strength of Newtonian gravity (e.g. Hu & Sawicki 2007; Nojiri & Odintsov 2011). However, it can be shown that, if $f(R)$ is chosen appropriately (Brookfield, van de Bruck & Hall 2006; Faulkner et al. 2007; Hu & Sawicki 2007; Li & Barrow 2007; Navarro & Van Acoleyen 2007; Brax et al. 2008), the model can exploit the so-called chameleon mechanism (Khoury & Weltman 2004; Mota & Shaw 2007) to suppress the gravity force enhancement and therefore pass the experimental constraints in high matter density regions such as our Solar system.

The basic idea of the chameleon mechanism is the following: the modifications to Newtonian gravity can be considered as an extra, or fifth, force mediated by the scalaron field f_R. Because the scalaron itself is massive, this extra force is of the Yukawa type, decaying exponentially $\exp(-mr)$, in which m is the scalaron mass, as the distance r between two test masses increases. In high matter density environments, m is very heavy and the exponential decay causes a strong suppression of the force over distance. In reality, this is equivalent to setting $|f_R| \ll 1$ in high-density regions because f_R is the potential of the fifth-force, and this leads to the GR limit as we have discussed above.

Consequently, the functional form of $f(R)$ is crucial in determining whether the fifth-force can be sufficiently suppressed in high-density environments. In this paper, we will focus on the $f(R)$ Lagrangian proposed by Hu & Sawicki (2007), for which

$$f(R) = -M^2\frac{c_1\left(-R/M^2\right)^n}{c_2\left(-R/M^2\right)^n + 1}, \quad (7)$$

where $M^2 \equiv 8\pi G\bar{\rho}_{\rm m0}/3 = H_0^2\Omega_{\rm M}$, with H being the Hubble expansion rate and $\Omega_{\rm M}$ the present-day fractional density of matter. Throughout this paper a subscript 0 always denotes the present-day ($a = 1$, $z = 0$) value of a quantity. It was shown by Hu & Sawicki (2007) that $|f_{R0}| \lesssim 0.1$ is necessary to evade the Solar system constraints but the exact constraint depends on the behaviour of f_R in galaxies as well.

In the background cosmology of this $f(R)$ model, the scalaron field f_R always sits close to the minimum of the effective potential that governs its dynamics, defined as

$$V_{\rm eff}\left(f_R\right) \equiv \frac{1}{3}\left(R - f_R R + 2f + 8\pi G\rho_{\rm m}\right), \quad (8)$$

around which it quickly oscillates with small amplitude (Brax et al. 2012). Therefore, we find

$$-\bar{R} \approx 8\pi G\bar{\rho}_{\rm m} - 2\bar{f} = 3M^2\left(a^{-3} + \frac{2c_1}{3c_2}\right). \quad (9)$$

To match the background evolution of the LCDM model which is tightly constrained nowadays (Hinshaw et al. 2012; Planck Collaboration 2013), we set

$$\frac{c_1}{c_2} = 6\frac{\Omega_\Lambda}{\Omega_{\rm M}}, \quad (10)$$

where $\Omega_{\rm M}$ and Ω_Λ are, respectively, the present-day fractional energy densities of the DM and dark energy.

We adopt standard LCDM model normalization, by taking $\Omega_\Lambda = 0.76$ and $\Omega_{\rm M} = 0.24$.[1] We find that $|\bar{R}| \approx 41M^2 \gg M^2$, and this simplifies the expression of the scalaron to

$$f_R \approx -n\frac{c_1}{c_2^2}\left(\frac{M^2}{-R}\right)^{n+1}. \quad (11)$$

Therefore, the two free parameters n and c_1/c_2^2 completely specify the Hu–Sawicki $f(R)$ model. Furthermore, c_1/c_2^2 is related to the value of the scalaron today, f_{R0}, by

$$\frac{c_1}{c_2^2} = -\frac{1}{n}\left[3\left(1 + 4\frac{\Omega_\Lambda}{\Omega_{\rm M}}\right)\right]^{n+1} f_{R0}. \quad (12)$$

[1] These values are used in the $f(R)$ simulations extensively in the literature, and we use them in the simulations used in this work in order to compare with previous work.

In this paper, we will study three $f(R)$ models with $n = 1$ and $|f_{R0}| = 10^{-6}, 10^{-5}$ and 10^{-4}, which we refer to as F6, F5 and F4, respectively. These choices of the value of $|f_{R0}|$ are decided to cover the whole parameter space that would be cosmologically interesting: if $|f_{R0}| > 10^{-4}$, then the $f(R)$ model violates the cluster abundance constraints (Schmidt, Vikhlinin & Hu 2009b), and if $|f_{R0}| < 10^{-6}$, then the difference from ΛCDM will be too small to be observable in practice, as we will show later.

3 THE *N*-BODY SIMULATIONS OF *f*(*R*) GRAVITY

From equations (5) and (6) we see that, with the matter density field known, we can solve for the scalaron field f_R using equation (5) and substitute the result into the modified Poisson equation (6) to solve for Φ. Once Φ is obtained, we can differentiate it to get the modified gravitational force which determines how the particles move in space. These are basically what we need to do in $f(R)$ N-body simulations to evolve the matter distribution.

The major challenge in $f(R)$ N-body simulations is to solve the scalaron equation of motion, equation (5), which is highly non-linear when the chameleon mechanism is at work. One way to do this is to use a mesh (or a set of meshes) on which f_R could be solved using, say, relaxation methods. This implies that mesh-based N-body codes are most convenient. On the other hand, tree-based codes are more difficult to apply here, as we do not have any analytical formula for the modified force law (such as the r^{-2}-law in the Newtonian case) due to the complexities stemming from the breakdown of the superposition principle.

We should also mention here that our treatment and modelling of the $f(R)$ gravity is done in the Newtonian limit for the $f(R)$ equations. This is a reasonable approximation as our simulations cover region of space that is much smaller than the horizon and peculiar velocities of all DM particles satisfy $v \ll c$.

N-body simulations of $f(R)$ gravity and related theories have previously been performed by Oyaizu (2008), Oyaizu, Lima & Hu (2008), Schmidt et al. (2009a), Zhao et al. (2011), Li & Zhao (2009, 2010), Schmidt (2009), Li & Barrow (2011), Brax et al. (2011) and Davis et al. (2012). As the strong non-linearity of equation (5) means that the code spends a significant portion of the computing time on solving it, most of these simulations were limited by either the box size or resolution, or both. For this work, we have run simulations using the recently developed ECOSMOG code (Li et al. 2012a). ECOSMOG is a modification of the mesh-based N-body code RAMSES (Teyssier 2002), which is efficiently parallelized using the message Passing Interface (MPI) and can therefore better utilize the supercomputing resources and improve on both simulation resolutions and box sizes. More technical details of the code can be found in Li et al. (2012a, 2013) and Jennings et al. (2012), and we will not repeat here.

The simulations used in this work are summarized in Table 1. All of them are described by the same set of cosmological parameters so that the background cosmology for all models is the same in practice (the difference caused by the different $f(R)$ model parameters is negligible). The values of cosmological parameters for our runs are the following: $\Omega_{\rm M} = 0.24$, $\Omega_\Lambda = 0.76, h = 0.73$, $n_{\rm s} = 0.958$ and $\sigma_8 = 0.80$, where $h \equiv H_0/(100\,{\rm km\,s^{-1}\,Mpc^{-1}})$ is the dimensionless Hubble parameter today, $n_{\rm s}$ is the scalar index of the primordial power spectrum and σ_8 is the linear rms density fluctuation measured in spheres of radius $8\,h^{-1}$Mpc at $z = 0$.

All models in each simulation share the same initial condition computed at the initial time of $z_{\rm i} = 49$ using the Zel'dovich approximation (Zel'Dovich 1970). Note that in general the modified gravity affects the generation of the initial condition too (Li & Barrow 2011), but in our case here we can use the same initial conditions for all three $f(R)$ models because the differences in clustering between GR and the $f(R)$ models are negligible at early times (redshifts higher than a few). The fact that we use the same initial conditions for all simulations in a given set is an advantage: since the initial density fields for the GR and $f(R)$ simulations have the same phases, any difference in the clustering amplitudes that we find at later times will be a direct consequence of the different dynamics between the two cosmologies.

3.1 Density estimation

We aim to compute higher order statistics of the density field. From the computation point of view, it is important to reconstruct high-resolution and high-quality density fields from the DM particles of our simulations. This is crucial for the accuracy of our later computations, as the high-order moments are strongly affected by shot noise and resolution effects. We choose to employ *the Delaunay Tessellation Field Estimator* method (hereafter DTFE) (Schaap & van de Weygaert 2000; van de Weygaert & Schaap 2009). We use the publicly available software implementing the DTFE method written by Cautun & van de Weygaert (2011). This approach consist of a natural method of reconstructing a volume-weighted and continuous density field from a discrete set of sampling points. The field reconstructed using the DTFE method is largely shot noise free down to the resolution limit (the fluid limit) of the point distribution. The shot noise is only present due to the intrinsic Monte Carlo sampling of the density inside the Delaunay cell. To suppress this source of error, we use 1000 Monte Carlo sampling points for each of the Delaunay tetrahedron. For our purpose, we decided to interpolate the DTFE density field over a 1024^3 regular sampling mesh. This sets our spatial resolution of 1.46 and $0.97\,h^{-1}$ Mpc for the 1500 and $1000\,h^{-1}$ Mpc box simulations, respectively. This is equal to the Nyquist scales for this simulations. For any discretely sampled field, the fluid limits breakdown close to its Nyquist scale/frequency. Thus, we will limit our analysis to the scales twice the resolution limit (respectively, 3 and $2\,h^{-1}$ Mpc).

Table 1. Some technical details of the simulations performed for this work. F6, F5 and F4 are the labels of the Hu–Sawicki $f(R)$ models with $n = 1$ and $|f_{R0}| = 10^{-6}, 10^{-5}$ and 10^{-4}, respectively. Here, $N_{\rm p}$ is the total number of N-body particles used and $k_{\rm Nyq}$ denotes the Nyquist frequency. Two parameters set the resolutions of our simulations, they are the force resolution ε and the mass resolution $m_{\rm p}$. The last column lists the number of realizations for each simulation.

Models	$L_{\rm box}$	$N_{\rm p}$	$k_{\rm Nyq}$ (h Mpc^{-1})	ε (h^{-1} kpc)	$m_{\rm p}$ (M$_\odot\,h^{-1}$)	Number of realizations
LCDM, F6, F5, F4	$1.5\,h^{-1}$ Gpc	1024^3	2.14	22.9	2.094×10^{10}	6
LCDM, F6, F5, F4	$1.0\,h^{-1}$ Gpc	1024^3	3.21	15.26	6.204×10^{9}	1

4 HIERARCHICAL CLUSTERING

4.1 The definitions

We start by introducing the DM density field, given by the expression

$$\rho(\boldsymbol{x}, t) = \langle\rho(t)\rangle\,[1 + \delta(\boldsymbol{x}, t)]\,, \tag{13}$$

where $\langle\rho(t)\rangle$ is the ensemble average of the DM density (the mean background density of the Universe) at time t, and $\delta(\boldsymbol{x}, t)$ (the local density contrast) describes local deviations from homogeneity. For clarity, we will drop the explicit time and position dependence of the density contrast in most of our equations. Structure formation is driven only by the spatially fluctuating part of the gravitational potential, $\phi(\boldsymbol{x}, t)$, induced by the density fluctuation field δ. In $f(R)$ cosmologies, however, we expect that in regions where the fifth-force is not screened by the chameleon mechanism; the standard gravitational potential will be enhanced by the scalaron as described by equation (6). Thus, we expect that clustering will be enhanced in our $f(R)$ models at small and moderate scales. This was already shown for the two-point statistics (Koivisto 2006; Li et al. 2013).

4.1.1 The cumulants of the density field

The non-linear gravitational evolution of the density field δ drives the field (and its distribution function) away from the initial Gaussian distribution. Deviations of a field from Gaussianity can be characterized by *cumulants* or *reduced moments*. Thus, the basic objects of our analysis are the cumulants of the density field distribution function $p(\delta)$. The nth cumulant of the distribution function δ is defined by recursive relation to the nth moments. This relation can be expressed by cumulant generating function (e.g. Łokas et al. 1995)

$$\langle\delta^n\rangle_{\rm c} \equiv M_n = \left.\frac{\partial^n \ln\langle {\rm e}^{t\delta}\rangle}{\partial t^n}\right|_{t=0}. \tag{14}$$

The cumulants now can be expressed in terms of the central moments, in particular, for the first nine cumulants we have (Bernardeau 1994; Gaztanaga 1994):

$$\begin{aligned}
\langle\delta\rangle_{\rm c} &= 0, \ \text{(the mean)}\\
\langle\delta^2\rangle_{\rm c} &= \langle\delta^2\rangle \equiv \sigma^2 \ \text{(the variance)},\\
\langle\delta^3\rangle_{\rm c} &= \langle\delta^3\rangle \ \text{(the skewness)},\\
\langle\delta^4\rangle_{\rm c} &= \langle\delta^4\rangle - 3\langle\delta^2\rangle_{\rm c}^2 \ \text{(the kurtosis)},\\
\langle\delta^5\rangle_{\rm c} &= \langle\delta^5\rangle - 10\langle\delta^3\rangle_{\rm c}\langle\delta^2\rangle_{\rm c},\\
\langle\delta^6\rangle_{\rm c} &= \langle\delta^6\rangle - 15\langle\delta^4\rangle_{\rm c}\langle\delta^2\rangle_{\rm c} - 10\langle\delta^3\rangle_{\rm c}^2 + 30\langle\delta^2\rangle_{\rm c}^3,\\
\langle\delta^7\rangle_{\rm c} &= \langle\delta^7\rangle - 21\langle\delta^5\rangle_{\rm c}\langle\delta^2\rangle_{\rm c} - 35\langle\delta^4\rangle_{\rm c}\langle\delta^3\rangle_{\rm c} + 210\langle\delta^3\rangle_{\rm c}\langle\delta^2\rangle_{\rm c}^2,\\
\langle\delta^8\rangle_{\rm c} &= \langle\delta^8\rangle - 28\langle\delta^6\rangle_{\rm c}\langle\delta^2\rangle_{\rm c} - 56\langle\delta^5\rangle_{\rm c}\langle\delta^3\rangle_{\rm c} - 35\langle\delta^4\rangle_{\rm c}^2\\
&\quad + 420\langle\delta^4\rangle_{\rm c}\langle\delta^2\rangle_{\rm c}^2 + 560\langle\delta^3\rangle_{\rm c}^2\langle\delta^2\rangle_{\rm c} - 630\langle\delta^2\rangle_{\rm c}^4,\\
\langle\delta^9\rangle_{\rm c} &= \langle\delta^9\rangle - 36\langle\delta^7\rangle_{\rm c}\langle\delta^2\rangle_{\rm c} - 84\langle\delta^6\rangle_{\rm c}\langle\delta^3\rangle_{\rm c} - 126\langle\delta^5\rangle_{\rm c}\langle\delta^4\rangle_{\rm c}\\
&\quad + 756\langle\delta^5\rangle_{\rm c}\langle\delta^2\rangle_{\rm c}^2 + 2520\langle\delta^4\rangle_{\rm c}\langle\delta^3\rangle_{\rm c}\langle\delta^2\rangle_{\rm c} + 560\langle\delta^3\rangle_{\rm c}^3\\
&\quad - 7560\langle\delta^3\rangle_{\rm c}^2\langle\delta^2\rangle_{\rm c}^3.
\end{aligned} \tag{15}$$

In general, the value of the nth cumulant is the value of the nth moment of the distribution from which one must subtract the results of all the decompositions of a set of n points in its subsets multiplied (for each decomposition) by the cumulants corresponding to each subset (Bernardeau 1994).

For the Gaussian field with a zero mean, all connected moments die out except the variance $\langle\delta^2\rangle$. In the classical random field theory, the first two non-vanishing cumulants after variance have special meaning as they measure particular shape departures of the distribution function from Gaussianity. The skewness is a measure of the asymmetry of the distribution and the value of kurtosis characterize the flattening of the tails with respect to a Gaussian. Higher cumulants measure more complicated shape deviations of the distribution function.

4.1.2 The hierarchical amplitudes

It is well established (e.g. Bernardeau 1992; Juszkiewicz et al. 1993; Gaztanaga & Baugh 1995; Szapudi et al. 1999; Bernardeau et al. 2002) that gravitational evolution of the initially Gaussian field creates and preserves quasi-Gaussian clustering hierarchy of cumulants that is characterized by the *hierarchical scaling*

$$\langle\delta^n\rangle_{\rm c} = S_n\langle\delta^2\rangle_{\rm c}^{n-1} = S_n\sigma^{2n-2}\,, \tag{16}$$

where the S_n are called *hierarchical amplitudes* or *reduced cumulants* and for unsmoothed field are constant. For example for $\Omega = 1$ Universe, Peebles (1980) found the reduced skewness to be $S_3 = 34/7 \cong 4.86$ while Bernardeau (1994) estimated the reduced kurtosis to be $S_4 = 60\,712/1223 \cong 45.89$.

4.1.3 The smoothing

The observational data stemming from recent and future galaxy redshift surveys allow one to estimate the cumulants of a *smoothed* density field. In order to make any testable predictions, we need to account for that fact. Thus, it is handy to define a new field $\overline{\delta}$, whose value at any point $\boldsymbol{x}$ in space is either the average value of δ in some defined volume, centred on $\boldsymbol{x}$, or an integral over volume, taken with some weighting function. Therefore, we define the smoothed density contrast field as

$$\delta_R(\boldsymbol{x}) \equiv \overline{\delta}(\boldsymbol{x}) = \int \delta(\boldsymbol{x}')W(|\boldsymbol{x} - \boldsymbol{x}'|/R_{\rm w}){\rm d}^3x'\,, \tag{17}$$

where $W(x/R_{\rm w})$ is a spherically symmetric window or smoothing function. We will consider only filters that are spherically symmetric with a finite effective half-width $R_{\rm w}$ and in addition are normalized to unity

$$\int W(y)\,{\rm d}^3y = 1 \quad \text{with} \quad \int W(y)y^2{\rm d}^3y = R_{\rm w}^2\,. \tag{18}$$

Smoothing over a ball of radius $R_{\rm TH} \equiv R_{\rm w}$ is called *top-hat* smoothing. We should denote here that effects of smoothing and gravitational dynamical evolution commute only for $\delta^1 = \delta$, for second and higher orders, these two processes are not interchangeable (see also Goroff et al. 1986; Juszkiewicz & Bouchet 1995).

It is convenient to define now the Fourier representation of the real density field. The Fourier space image of a density field is

$$\delta(\boldsymbol{k}) \equiv (2\pi)^{-3/2}\int \delta(\boldsymbol{x})\,{\rm e}^{-{\rm i}\boldsymbol{k}\cdot\boldsymbol{x}}\,{\rm d}^3x\,. \tag{19}$$

The main advantage of the frequency space is that a convolution of real-space functions from equation (17) is exchanged by a simple multiplication. In Fourier space, the smoothed density contrast is then

$$\delta_R(\boldsymbol{k}) = \delta(\boldsymbol{k})W(\boldsymbol{k}R_{\rm TH})\,, \tag{20}$$

where

$$W(\boldsymbol{k}R_{\rm TH}) = (2\pi)^{-3/2} \int W(\boldsymbol{x}/R_{\rm TH})\, {\rm e}^{-{\rm i}\boldsymbol{k}\cdot\boldsymbol{x}}\, {\rm d}^3x \tag{21}$$

is the Fourier image of the window function. For the spherical top-hat window that we use the transformation yields $W(\boldsymbol{k}R_{\rm TH}) = (3/kR_{\rm TH})j_1(kR_{\rm TH})$ with j_1 being a spherical Bessel function of the first kind. Now, if we want to obtain a smoothed real-space density field δ_R, we can employ the top-hat filtering in Fourier space and use inverse transformation to get back the top-hat smoothed real-space field

$$\delta_R(\boldsymbol{x}) = (2\pi)^{-3/2} \int \delta_R(\boldsymbol{k}) W(\boldsymbol{k}R_{\rm TH})\, {\rm e}^{{\rm i}\boldsymbol{k}\cdot\boldsymbol{x}}\, {\rm d}^3k. \tag{22}$$

We will use this technique extensively in our studies as it is very efficient computationally. Finally, we can define *volume-averaged* n-point correlation function of the field δ_R as

$$\overline{\xi}_n(R_{\rm TH}) \equiv \langle\delta_R^n\rangle_{\rm c} = \int {\rm d}^3x_1, \ldots, {\rm d}^3x_n \xi(\boldsymbol{x}_1, \ldots, \boldsymbol{x}_n) W(x_1/R_{\rm TH}), \ldots, W(x_n/R_{\rm TH}). \tag{23}$$

The effects of smoothing on hierarchical amplitudes and density cumulants were studied within a perturbation theory (hereafter PT) framework by Bernardeau (1994) and Juszkiewicz et al. (1993). They both found that smoothing induces weak scale dependence of the S_n and this effect is quantified by various combinations (depending on the cumulant order) of the logarithmic slope of the variance γ_n, which is defined as

$$\gamma_n(R_{\rm TH}) \equiv \frac{{\rm d}^n \log\sigma^2(R_{\rm TH})}{{\rm d}\log^n R_{\rm TH}}. \tag{24}$$

For a smoothed reduced skewness S_3 and kurtosis S_4, the PT predicts (Bernardeau 1994)

$$S_3 = \frac{34}{7} + \gamma_1,$$
$$S_4 = \frac{60\,712}{1323} + \frac{62}{3}\gamma_1 + \frac{7}{3}\gamma_1^2 + \frac{2}{3}\gamma_2. \tag{25}$$

For a density field characterized by the spectral index $-3 \leq n \leq 1$, the values of the logarithmic slope will take $\gamma_n \leq 0$ (Juszkiewicz et al. 1993). Hence, smoothing decreases values of S_n. Thus, assuming that PT results of these authors would also hold for $f(R)$ and all modified gravity effects would be encoded in the modified slope of the variance, we can expect that the hierarchical amplitudes will be sensitive to the enhanced matter clustering exhibited by the $f(R)$ models.

4.1.4 The estimation of moments

The study presented in this paper will concern the smoothed DM density fields. Having this in mind, we have decided to design and use a special, yet simple and fast algorithm for computing the moments of the δ_R field. It can be summarized in a following few steps.

(i) Obtain the initial density field δ on a uniform grid from a simulation snapshot using the DTFE method. This sets our limiting spatial resolution to the size of the grid cell. We interpolate the DTFE matter density field on to regular $N_{\rm g} = 1024^3$ cubical cells grid.

(ii) Perform a forward *fast Fourier transform* (FFT) of the field. Multiply the $\delta(\boldsymbol{k})$ field values with the Fourier top-hat window for a chosen value of $R_{\rm TH}$.

(iii) Perform a backward FFT to obtain the smoothed real density field δ_R.

(iv) Compute central moments of the distribution function using

$$\langle\delta_R^n\rangle = \frac{1}{N_{\rm g}} \sum_i^{N_{\rm g}} \left(\delta_R^i - \langle\delta_R\rangle\right)^n. \tag{26}$$

(v) Finally, we use equations (15) to obtain the cumulants of the input field smoothed at scale $R_{\rm TH}$.

By applying this algorithm to our simulation data we get the first nine cumulants of the density field for a range of smoothing scales. We have to note that while we always use the initial number of field components $N_{\rm g}$ for each smoothing scale $R_{\rm TH}$, it is evident that with increasing scale more and more cells will become correlated. Thus, we are limited by the finite volume effects at large scales, which becomes severe for scales $R_{\rm TH} \gtrsim 0.1L_{\rm box}$ (Colombi, Bouchet & Schaeffer 1994). At the same time, we are also limited by the Nyquist sampling limit or the initial grid spacing at small scales. Hence, for the purpose of our analysis, we will only consider scales that satisfy $2/\sqrt[3]{N_{\rm g}} < R_{\rm TH}/L_{\rm box} < 0.1$, where $N_{\rm g}$ is the number of the grid cells (set to be the same as the number of DM particles) and the $L_{\rm box}$ is the comoving width of the simulation box.

The algorithm described above provides a very fast and parallelized method for obtaining higher order cumulants from a given initial density field. We have thoroughly tested the code implementing our algorithm by comparing results with the usual spherical counts-in-cells methods (e.g. Bouchet & Hernquist 1992; Gaztanaga & Baugh 1995). For the modified gravity simulation data presented in (Hellwing et al. 2010), we have found perfect agreement with the results both for GR and for modified gravity.

4.1.5 Sampling errors

In this work, we focus on a direct comparison of the non-linear clustering amplitudes between the GR (LCDM) and $f(R)$ cosmologies. In order to make the comparison, we need to quantify the variance or the sampling errors of our measurements. The variance of a count-in-cells estimator of a cumulant of an nth order, in general, depends on values of cumulants of $n+2$ and $n+1$ order (Kendall & Stuart 1977). For example, the variance of the second cumulant (the field variance itself) is estimated by

$${\rm var}\left[\langle\delta^2\rangle_{\rm c}\right] = N_{\rm g}^{-1}\left(\langle\delta^4\rangle_{\rm c} - 2\langle\delta^3\rangle_{\rm c} + \langle\delta^2\rangle_{\rm c} - \langle\delta^2\rangle_{\rm c}^2\right). \tag{27}$$

In practice however the above estimator is rather cumbersome to use. This is because the high-order cumulants are more severely affected by the finite volume effects (e.g. Hellwing et al. 2010); this effect will render equation (27) unusable for cumulants of order $n \geq 5$ for scales larger than $\sim 20\,h^{-1}$ Mpc. For that reason, we decided to use the variance of the measured cumulants coming from ensemble averaging as our main error estimator. This is a reasonable approach, as the errors coming from averaging between different realizations of the initial conditions are more conservative than the estimator of equation (27) (Baugh et al. 1995; Hellwing et al. 2010). To validate that we plot Fig. 1, where we compare two standard deviation relative error $(\sigma_{\overline{\xi}_2}/\overline{\xi}_2)$ estimators for $\overline{\xi}_2$. The red line marks the relative error estimated using equation (27), while with the blue line we draw the appropriate error estimated from ensemble averaging. The plot clearly demonstrates that the ensemble average

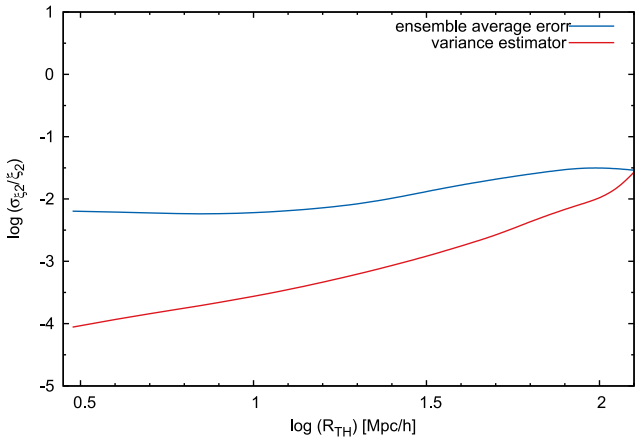

Figure 1. Comparison of two relative error estimators ($\sigma_{\bar{\xi}_2}/\bar{\xi}_2$) for the $\bar{\xi}_2$ cumulant for the GR ensemble for 1500 h^{-1} Mpc box. The red line depicts the square root of variance estimator from equation (27), while the blue line marks the dispersion coming from ensemble average of the six different realizations.

error is conservative for all probed smoothing scales and that the both estimators converge at large scale as expected.

4.1.6 Transients

We would like also to discuss briefly another possible source of error in form of artificially induced bias coming from the procedure used to generate the initial conditions for our simulations. As mentioned before, we use the Zel'dovich approximation to obtain the displacement field that is used to compute particles' peculiar velocities and displace particles from their initial Eulerian coordinates. Because the Zel'dovich procedure does not conserve momentum, the density distribution function of a field generated using this technique possess a non-vanishing artificial skewness, kurtosis and higher order cumulants. This unwanted and unphysical deviations from the true dynamics are called *transients* and have been studied in detail in the literature (e.g. Scoccimarro 1998; Crocce, Pueblas & Scoccimarro 2006; Tatekawa & Mizuno 2007). To eliminate the effect of transients from initial conditions a system must be allowed to evolve in a pure dynamical way for a sufficiently long time. The effects of transients for general class of models with scalar field induced fifth-force was studied by Hellwing et al. (2010). Their study implies that transients effects can be of the order of a few per cent (∼5–10 per cent) for the skewness at scales where the unscreened fifth-force is allowed to act ($R_{\rm TH} \leq 1\,h^{-1}$ Mpc in their models).

Because of the above, the initial redshift of a cosmological simulation is an important factor in determining the statistical reliability of the cosmological numerical experiment. In general, for the purpose of comparison of density fields and cumulants in different models, we need to be less concerned about the net amplitude of the transients as they will have the same magnitude in all models. This is because in the $f(R)$ class of models we consider, the scalar field and the fifth-force have negligible effects for the matter fields dynamics until redshifts of a few, for $z \gtrsim 4$ (e.g. Oyaizu et al. 2008; Li et al. 2013) the growth and expansions histories are closely matched between GR and $f(R)$. Therefore, before the fifth-force will start to change the dynamic of the density field evolution the transients will be largely erased thanks to moderately high starting redshift of our simulations.

5 RESULTS

In this section, we present analysis and discussion of main results of our study. First, we focus on $z = 0$ density field and its cumulants hierarchy. Then, our analysis is followed by a detailed study of the redshift evolution of the $f(R)$ gravity effects in the clustering of the matter.

5.1 The variance and the σ_8

First, we look at the variance of the density field in our models. The two-point statistic for $f(R)$ gravity was studied both using numerical simulations (Oyaizu et al. 2008; Li & Barrow 2011; Zhao et al. 2011; Li et al. 2013) and PT (Bean et al. 2007; Li & Barrow 2007; Song, Hu & Sawicki 2007). The results in the literature mostly focus on the power spectrum of the density fluctuations $P(k) \equiv \langle \delta_k^2 \rangle$. The variance of a field is related to its Fourier power spectrum by

$$\sigma^2(R_{\rm TH}) = \int \frac{{\rm d}k}{2\pi^2} k^2 P(k) W_{\rm TH}^2(k R_{\rm TH})\,. \tag{28}$$

Here, $W_{\rm TH}$ is the Fourier top-hat window described by equation (21) and $R_{\rm TH}$ is the comoving smoothing scale in h^{-1} Mpc. In cosmology, the variance of the density field plays a special role via the σ_8 parameter. The σ_8 is the square root of the density field variance smoothed with $8\,h^{-1}$ Mpc top-hat. The linear theory prediction for the σ_8 is employed as a normalization parameter for the power spectrum and is extensively used for generation of initial conditions for cosmological numerical simulations. The scale of $8\,h^{-1}$ Mpc is chosen as, in principle, for most viable cosmological models this scale separates non-linear density perturbation regime ($\delta \gg 1$) from the linear one ($\delta < 1$). In practice, however, these two regimes are combined by mildly non-linear regime where $\delta \sim O(1)$. Due to existence of this intermediate regime, some mode coupling occurs and the value of the density variance at $8\,h^{-1}$ Mpc at late times is affected by mildly non-linear evolution. Hence, the value of σ_8 measured in cosmological N-body simulations as well as in astronomical observations is higher than the linear theory prediction (for an excellent discussion see Juszkiewicz et al. 2010). We expect that the impact of weakly non-linear dynamics on the variance and the value of the σ_8 parameter in particular, will be pronounced in the $f(R)$ gravity models. This is because, as many authors have shown, the amplitude of the density power spectrum in $f(R)$ theories is increased as compared to GR for wave numbers $k \gtrsim 0.1\,h\,{\rm Mpc}^{-1}$. To check how big is the effect of the scalaron for the real-space density variance we present Fig. 2. The top panel shows the variance $\langle \sigma^2 \rangle$ of a field smoothed over a range of scales and averaged over ensemble of six realizations of the $1500\,h^{-1}$ Mpc simulations. The bottom panel illustrates the relative deviation of the $f(R)$ gravity models from the values of the fiducial GR case. We define this relative deviation as

$$\Delta\sigma^2 \equiv \frac{\sigma^2_{f(R)}}{\sigma^2_{\rm GR}} - 1\,. \tag{29}$$

The lines representing different models are: black for GR, red for F4, blue for F5 and green for F6. We will use this colour scheme throughout the paper to present our results. The black vertical dot–dashed line marks the $R_{\rm TH} = 8\,h^{-1}$ Mpc scale, whilst the shaded region represents the 1σ scatter around GR ensemble mean (invisible on the top panel due to smallness of the errors). Looking at both the panels, we clearly see that the variance is enhanced in $f(R)$ for a range of smoothing scales. As expected, the F6 model shows weakest deviations, while the F4 exhibits strong enhancement of the clustering amplitude. For the latter, we can observe that even at

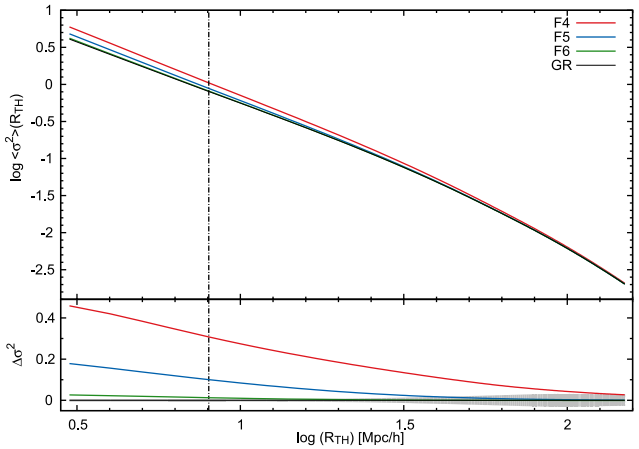

Figure 2. The average variance $\langle\sigma^2(R_{\rm TH})\rangle$ of the density field for GR and three flavours of $f(R)$ gravity for 1500 h^{-1} Mpc ensembles. Vertical dot–dashed line marks the smoothing scale $R_{\rm TH} = 8\,h^{-1}$ Mpc. The shaded region represents 1σ scatter over ensemble.

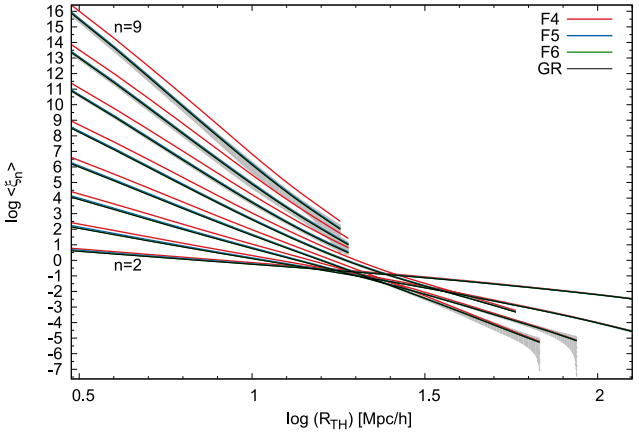

Figure 3. The averaged n-point correlation functions $\langle\bar{\xi}_n\rangle$ for a range of smoothing scales. At smallest smoothing scale, the lines can be clearly distinguished by the increasing amplitude, starting from $\langle\bar{\xi}_2\rangle$ for the lowest line, up to $\langle\bar{\xi}_9\rangle$ for the highest amplitude. Shaded regions mark 1σ errors around the GR mean. We plot functions only out to the scales which are not yet strongly affected by the noise and finite volume effects.

scales $R_{\rm TH} \sim 100\,h^{-1}$ Mpc the value of $\Delta\sigma^2$ is of the order of ∼0.05. To allow for a better comparison between models we show Table 2. There, we examine the values of averaged standard deviation for a few chosen smoothing scales. At $R_{\rm TH} = 3\,h^{-1}$ Mpc, the resolution scale of our $1500\,h^{-1}$ Mpc simulations, the modified gravity effects are large for both F4 and F5. The F6 model at this scale shows only 1 per cent enhancement of clustering amplitude. For the F5 model, values of $\langle\sigma(R_{\rm TH})\rangle$ quickly converge to GR for scales $R \geq 20\,h^{-1}$ Mpc; however, the F4 model variance bears significant signal even at 50 and $100\,h^{-1}$ Mpc scales. This is emphasized by the fact that the value of non-linear σ_8 for this model is in 14 per cent excess from GR as $\sigma_8^{\rm GR} = 0.9$ and $\sigma_8^{\rm F4} = 1.03$. This result could in principle be measurable, as observational data provide estimate of the non-linear σ_8 parameter. However, for the most of the data available for σ_8, to be properly interpreted within $f(R)$ framework, would require some assumed model of the galaxy biasing in $f(R)$ gravity. We will address this issue in a forthcoming paper (Hellwing et al., in preparation). Here, we can comment that some estimates of the σ_8 parameter based on peculiar velocities (hence largely independent on galaxy biasing) favour high value of this observable. For example, Feldman et al. (2003) using pairwise velocities method estimate it to be $\sigma_8 = 1.13^{+0.22}_{-0.23}$, while Watkins, Feldman & Hudson (2009) by assessing the bulk flow in local universe got $\sigma_8 > 1.11$ at 95 per cent CL. Both velocity-based estimates are in slight tension with galaxy-clustering measurements that usually yield lower value of the normalization parameter $\sigma_8^{\rm gal} = 0.92 \pm 0.06$ (Tegmark et al. 2004; Cole et al. 2005; Eisenstein et al. 2005). However, to allow for a fair comparison with observations, both methods need to be corrected for the $f(R)$ framework. The velocity-based methods must account for additional accelerations induced by the fifth-force in unscreened parts of the Universe, while the galaxy-clustering method need to be corrected for realistic galaxy formation and biasing in $f(R)$. Both issues are subject of our work in progress and will be presented in a forthcoming paper.

5.2 *n*-point functions and hierarchical amplitudes

We move to higher order correlation functions (cumulants) hierarchical amplitudes that constitute the main subject of our study.

5.2.1 *General properties*

First, we take a look at the whole family of eight correlation functions from $\bar{\xi}_2$ to $\bar{\xi}_9$ and associated with them seven hierarchical amplitudes from reduced skewness S_3 up to S_8. We plot them on Figs 3 and 4, respectively. For every GR line, we also draw a shaded region that marks the 1σ scatter around the mean value from ensemble. We note that for small and intermediate smoothing scales $3\,h^{-1}$ Mpc $\leq R_{\rm TH} \lesssim 20\,h^{-1}$ Mpc in the regime of modified $f(R)$ gravity, the amplitudes of volume-averaged correlation functions exhibit excess when compared to the fiducial GR case. This is especially clearly seen for the F4 model. Exactly opposite effect can

Table 2. The value of $\langle\sigma(R_{\rm TH})\rangle^{0.5}$ for a chosen smoothing scales $R_{\rm TH}$. We do not show the values of 1σ errors from averaging, as for small scales they are <1 per cent and reach only ∼3 per cent for $R_{\rm TH} = 100\,h^{-1}$ Mpc. The percentage values given in parentheses are relative deviations from the GR case, as defined in equation (29).

Smoothing scale	$\langle\sigma^2(R_{\rm TH})\rangle^{0.5}$			
$R_{\rm TH}$ (h^{-1} Mpc)	GR	F4	F5	F6
3	2.02	2.44 (21 per cent)	2.19 (9 per cent)	2.05 (1 per cent)
8	0.9	1.03 (14 per cent)	0.94 (5 per cent)	0.9 (0.7 per cent)
20	0.42	0.45 (7 per cent)	0.43 (2 per cent)	0.42
50	0.173	0.181 (5 per cent)	0.175 (1 per cent)	0.173
100	0.078	0.08 (3 per cent)	0.078	0.078

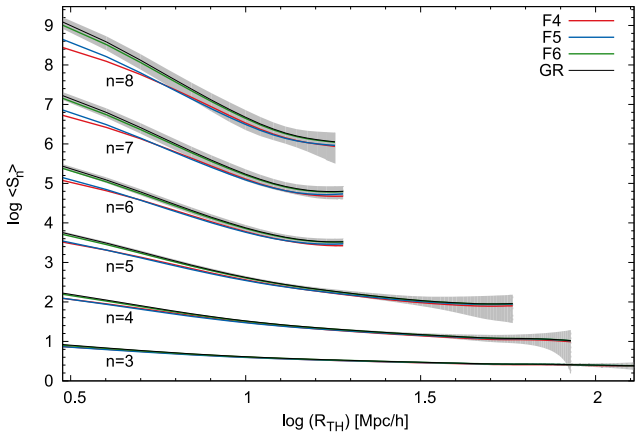

Figure 4. As in Fig. 3, but this time hierarchical amplitudes $\langle S_n \rangle$ are displayed. Here, the lines start from the lowest order $n = 3$ which marks the reduced skewness S_3 and are plotted for sequentially increasing order of the hierarchical amplitude up to $n = 8$.

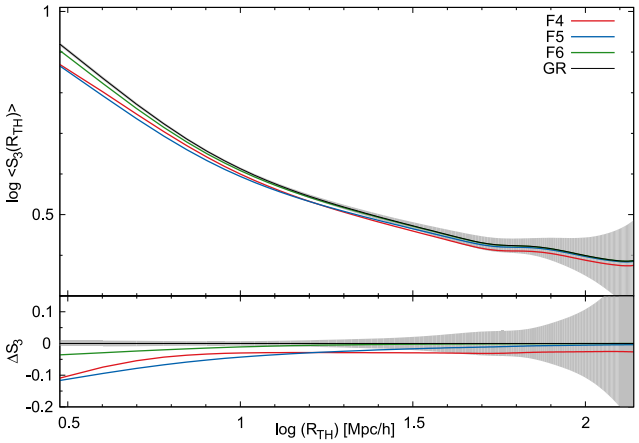

Figure 5. The averaged reduced skewness $\langle S_3 \rangle$ from $1500\,h^{-1}$ Mpc ensembles. The solid colour lines depict ensembles: GR (black), F4 (red), F5 (blue) and F6 (green). The lower panel presents the relative difference ΔS_3 from the GR case. The shaded area illustrate 1σ scatter around the ensemble mean for the GR simulations.

be seen for the hierarchical amplitudes. Here, we observe that the density field in $f(R)$ models is characterized by lower values of the S_n functions compared to the GR Universe. We can also note that the relative differences between modified gravity and GR get bigger and bigger as we move to higher and higher order amplitudes. For S_8, the differences at $3\,h^{-1}$ Mpc can be as big as a factor of a few. Fig. 4 also illustrates the important fact, namely that in the case of $f(R)$ gravity the quasi-Gaussian correlation hierarchy is also present just as for the standard GR model, the main difference being that the amplitudes and their scale dependence deviate from the standard model.

This preliminary analysis implies that we can expect to see strong modified gravity signal in the hierarchical amplitudes at small scales, and we can expect that the relative deviation from the GR case gets stronger for higher orders. Another important observation we would like to emphasize here regards the fact that lower values of the $f(R)$ hierarchical amplitudes actually mean that their density distribution functions are departing from their GR equivalents. We will discuss the physical interpretation of this observation later on.

5.3 The skewness, kurtosis and S_5

From the observational point of view, higher order clustering amplitudes are harder to measure and are no doubt affected by larger uncertainties. The cumulants that are most studied for the standard gravity paradigm are skewness and kurtosis. We include also S_5 in this set and focus our analysis on these three first measures of the deviation from Gaussianity. Three-point correlations have previously been studied for modified gravity models. Bernardeau (2004) and Borisov & Jain (2009) studied the bispectrum, while Tatekawa & Tsujikawa (2008) derived the formula for the modified gravity skewness of the density field in a matter-dominated (Einstein–de Sitter) Universe approximation. The former works find the reduced bispectrum of the modified gravity to deviate only very weakly from the GR case. For example, Borisov & Jain (2009) for the F4 model find deviation of the reduced bispectrum amplitude for $k \gtrsim 0.1\,h\,\mathrm{Mpc}^{-1}$ to be only of the order of $\sim$1 per cent. Analogously, Tatekawa & Tsujikawa (2008) find deviation (lower value than in the GR) in the reduced skewness to be at best of the order of $\sim$2 per cent for a strongly coupled scalar field. Both results were obtained using PT that includes second-order terms. The validity of such approach was largely tested for the three-point statistic in the GR universe. Surprisingly, many authors (e.g. Juszkiewicz et al. 1993; Bouchet et al. 1995; Gaztanaga & Bernardeau 1998) found good agreement with N-body simulations also in the regime where weakly non-linear PT should fail, i.e. $\delta \sim 1$. However, as we will see later on, this approach fails for the modified gravity models. First of all the class of the modified gravity theories and the $f(R)$ models we study here, in particular, are characterized by the higher degree of non-linearity. This is due to stronger clustering as showed by us for the case of variance in Section 5.1, but also the highly non-linear character of the evolution and distribution of the chameleon field adds to the total degree of non-linearity of the density field. Secondly, the PT is limited and ill-posed to look for the modified gravity signatures in the δ field, as these signatures are strongest at small scales, which by construction are beyond the validity of the perturbation regime.

In Fig. 5, we plot the real-space skewness obtained from the $1500\,h^{-1}$ Mpc ensemble. The top panel shows the absolute value of the S_3 for the field smoothed at a range of scales $3-150\,h^{-1}$ Mpc. The bottom panel illustrates the relative deviation from the GR values ΔS_3, defined in the analogous way as in equation (29). As usual, the shaded regions quantify the 1σ deviations from the GR mean. In connection with the above-mentioned results of other authors, we indeed confirm that at large scales $R_{\mathrm{TH}} \gtrsim 40\,h^{-1}$ Mpc both F5 and F6 models converge to the GR case. However, this is not the case for the F4 model. The skewness in this model bears the signal of modified dynamics at level of $\sim$5 per cent from 10 up to $100\,h^{-1}$ Mpc. We also find that there is regime of strong deviation of $f(R)$ gravity clustering from the Einstein theory case. It appears for the scales $\leq 10\,h^{-1}$ Mpc. We find the strongest signal at the resolution limit $R_{\mathrm{TH}} = 3\,h^{-1}$ Mpc of our $1500\,h^{-1}$ Mpc box simulations. Here, $\Delta S_3 = -12$ per cent both for F4 and F5 models and is still of the order of -4 per cent for the F6 case. We would like also to make a side remark on this occasion. In our S_3 data, we have found the baryon acoustic oscillations (BAO) signal for all models at scales predicted by Juszkiewicz, Hellwing & van de Weygaert (2013) and Hellwing et al. (2013). The wiggle can be clearly seen in Fig. 5 for scales $1.5 < \log(R_{\mathrm{TH}}) < 2$.

The mark of modified gravity is further enhanced in the case of the kurtosis and the fifth-order amplitude S_5. We plot corresponding

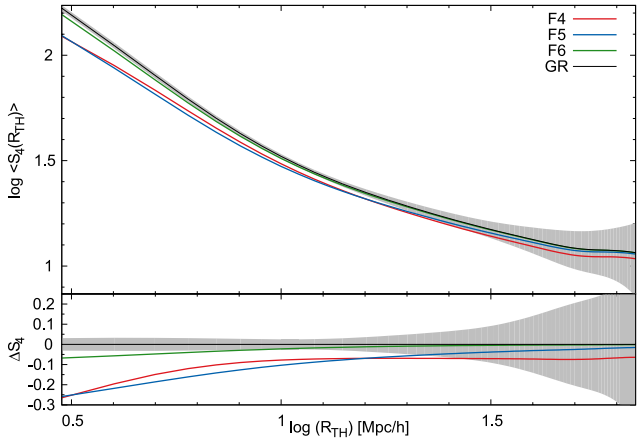

Figure 6. The averaged kurtosis $\langle S_4 \rangle$ from $1500\,h^{-1}$ Mpc ensemble. The definitions of lines and panels are the same as in Fig. 5.

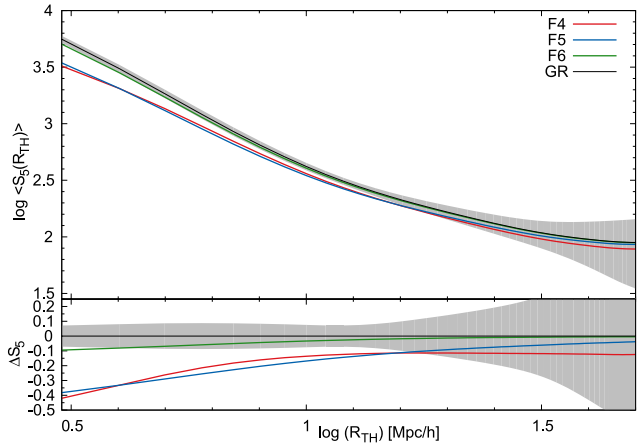

Figure 7. The averaged $\langle S_5 \rangle$ from $1500\,h^{-1}$ Mpc ensemble. The definitions of lines and panels are the same as in Fig. 5.

data on Figs 6 and 7. For our limiting radius of $3\,h^{-1}$ Mpc, the relative deviation from the fiducial GR case reaches $\Delta S_4 = -26$ per cent and $\Delta S_5 = -42$ per cent, respectively. Furthermore, the statistical significance of the measured deviations is very big. For the $R_{\rm TH} = 3\,h^{-1}$ Mpc, the F4 mean values are 11, 8.5 and 6.9σ away from the GR mean for S_3, S_4 and S_5, respectively. This means that in statistical sense the density field at those scales is characterized by different shape density distribution functions for each of our models. For a better comparison, we have collected the values of measured S_3, S_4 and S_5 for a few chosen smoothing scales in Table 3.

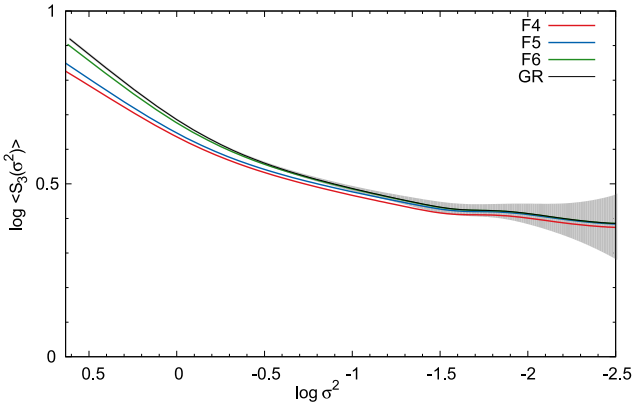

Figure 8. As Fig. 5, but this time the averaged skewness is plotted against averaged field variance $\langle \sigma^2 \rangle$.

Closer inspection of the data plotted in Figs 5–7 reveals an interesting feature. It appears that for the scales below $\sim 10\,h^{-1}$ Mpc the relative deviation is *stronger* for the F5 model than for F4 model. At our resolution limit both signals seem to converge to a similar value. However, for the mentioned scales the hierarchical amplitudes of the F5 density field are smaller than for any other considered models. To better understand this behaviour, we show Fig. 8, where the skewness is plotted against variance σ^2 of the field rather than smoothing scale. The plot shows that for all values of the variance, the lowest skewness belongs to the F4 model, as we would initially expect. At small scales, for the same smoothing radius it is the F4 model that has the largest variance. Hence, the lines from Fig. 5 get shifted accordingly. For the general class of the fifth-force cosmology, Hellwing et al. (2010) found that the stronger the fifth-force or larger screening length the stronger the deviation in the S_n functions. This is apparently not the case for our F5 and F4 models. We can propose the following explanation of this phenomena. In generic flavours of modified gravity models, the fifth-force is allowed to act freely on all the scales of interest for a particular model. Thus, once the force arises due to non-minimal coupling of the scalar field to matter it changes the dynamics of the matter field. In realistic family of such models, the fifth-force is usually suppressed for large scales and can only act on small and intermediate scales. Therefore, an unavoidable quality of a model without environment-dependent screening is that the effects of modified gravity are strongest at small scales. Now if we consider our *f*(*R*) models, we need to take into account the chameleon mechanism that is screening out the fifth-force in dense parts of the field.

Now we can naturally explain the unexpected behaviour of the S_n functions for the F4 and F5 models. The F4 model is the one that experiences the strongest clustering. As mentioned before, it has the

Table 3. The values of averaged hierarchical amplitudes for $n = 3$, 4 and 5 presented here for a few chosen smoothing radii. Each column contains four comma-separated numbers. The first one (black) gives the GR mean plus error, the second (red) is for the F4 model, the third (blue) corresponds to F5 and finally the fourth (green) represents F6.

Smoothing scale $R_{\rm TH}$ (h^{-1} Mpc)	S3	S4 GR,F4,F5,F6	S5
3	8.31 ± 0.08, 7.4, 7.34, 8.01	167.2 ± 5.2, 123, 124, 156	5661 ± 403, 3269, 3491, 5123
8	4.53 ± 0.03, 4.38, 4.3, 4.47	42.5 ± 1.2, 38.7, 37.1, 41.2	643 ± 54, 540, 512, 615
20	3.3 ± 0.04, 3.21, 3.22, 3.29	19.2 ± 0.9, 17.9, 18.1, 19.1	165 ± 23, 146, 150, 163
50	2.7 ± 0.1, 2.61, 2.67, 2.69	12.2 ± 2.5, 11.2, 11.9, 12.1	89 ± 54, 78, 86, 89
100	2.51 ± 0.27, 2.44, 2.49, 2.51	9.5 ± 17.2, 8.7, 9.3, 9.4	–, –, –, –

non-linear $\sigma_8^{F4} = 1.03$, which should be compared with ∼9 per cent lower value of the F5 model $\sigma_8^{F5} = 0.94$. Due to stronger clustering and more efficient matter accretion, cluster mass haloes get more massive (Schmidt et al. 2009a). In general, we can expect that, on average, the small-scale matter aggregations like clusters and filaments will be denser in the F4 model when compared to F5. In addition, in the F4 model, the chameleon screening is much less effective when compared to the F5 universe. Hence, while both F4 and F5 models experience fifth-force enhanced dynamics in low-density environments like cosmic voids and walls, the fifth-force in the F5 model is partially screened out in dense cluster and filaments. This naturally leads to stronger deviation in the hierarchical amplitudes at small scales. To conclude, what we observe in the behaviour of the S_3, S_4 and S_5 values shown in Figs 5–7 is the chameleon mechanism caught in the act during large-scale structure formation in $f(R)$ gravity models.

5.4 The redshift evolution

So far we have focused on the $z = 0$ results of our simulations. From physical, but also observational point of view, it is important to study the time evolution of the high-order correlation hierarchy. The hierarchical structure formation paradigm that is a part of the CDM model assumes that structures in the Universe arise from primordial tiny Gaussian-distributed density fluctuations by means of the gravitational instability mechanism. In this picture, the high-redshift density distribution function is closer to a Gaussian, and as the system is evolving in time, the gravitational dynamics drives the density field far away from the initial Gaussian distribution. The prediction is that the skewness and higher order amplitudes grow with time at scales where the non-linear and mildly non-linear evolution occurs (see e.g. Guillet, Teyssier & Colombi 2010). Since we know that in the $f(R)$ cosmology the density field experiences a modified (enhanced) density perturbation growth history, we also expect that the pattern of growth in time of the hierarchical amplitudes will be modified w.r.t. the GR case. We begin by looking more closely at the time evolution of the skewness for the GR model. In Fig. 9, we plot the averaged smoothed skewness for the GR $1000\,h^{-1}$ Mpc box simulation at nine different time steps. The lines are coloured according to redshift with the reddest marking the highest redshift $z = 4$ and the bluest pointing to $z = 0$. In the considered redshift range, we observe that the values of the skewness converge for $R_{TH} \geq 35\,h^{-1}$ Mpc. However, at smaller scales a much higher positive skewness develops with time. This effect is of course driven by non-linear gravitational evolution, namely collapse of DM haloes and emptying of cosmic voids. Here, at $R_{TH} = 2\,h^{-1}$ Mpc the skewness doubles its value from $S_3 = 4.9$ to 9.5 between $z = 4$ and 0. We also denote that the fastest growth of the skewness appears at earlier times, for $z > 1.5$. Below this redshift the skewness grows much slower.

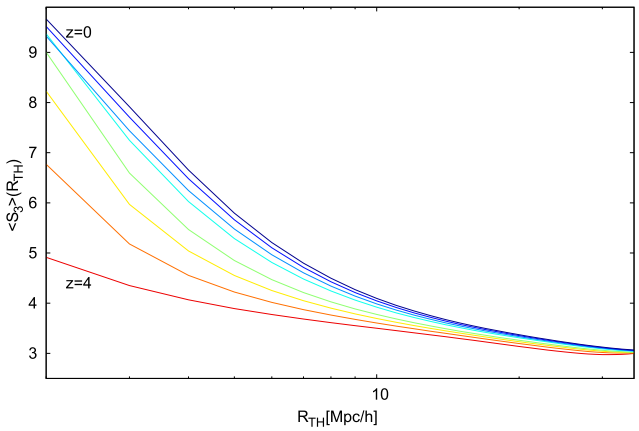

Figure 9. Gravitational instability at work. The redshift evolution of the skewness for the GR model in $1000\,h^{-1}$ Mpc box. The lines from bottom (red) to top (yellow) mark snapshots taken at consecutive redshifts: 4, 2.33, 1.5, 1, 0.43, 0.25, 0.1 and 0.

Once we have established what the time evolution of the skewness looks like, for the LCDM model we are now ready to quantify the redshift evolution of the relative deviations of the $f(R)$ skewness, kurtotsis and S_5 from the standard gravity model predictions. This is illustrated by Fig. 10, where we plot the time evolution of ΔS_3, ΔS_4 and ΔS_5 for the F4, F5 and F6 models. The three columns of this figure correspond to our three flavours of the $f(R)$, from F4 (the leftmost columns) to F6 (the rightmost column), while the different rows present consecutive hierarchical amplitude deviations from ΔS_3 in the top row to ΔS_5 presented at the bottom row. We start our analysis by looking at the F5 and F6 models, putting aside the strongest F4 case for the moment, as it experiences the most complicated time evolution. Again, the lines are coloured according to the corresponding redshift, starting from the $z = 4$ for the reddest line down to $z = 0$ marked by the bluest colour. First, we denote that the F6 model data look like a weaker and retarded in time version of the F5 model. General trends are the same for both models. The deviations from the GR density field undergo the fastest evolution for $1 \lesssim z \leq 4$. At redshift ∼0.6 most of the differences between the F5, F6 and the GR Universes are already in place and for the remaining expansion history of the Universe the deviations of both models' hierarchical amplitudes grow only weakly. These tendencies are somewhat similar also for the F4. Here, though we observe a development of a very interesting pattern of deviations in time and scale. First of all, we observe that the ΔS_n functions are no longer monotonic with time and scale. While the deviations are still strongest at small, non-linear, scales $R_{TH} \leq 10\,h^{-1}$ Mpc, we see that for the scales $10 \lesssim R_{TH}/\,h^{-1}$ Mpc $\lesssim$ 50–60 the actual values of the ΔS_n grow slowly with the scale. This behaviour occurs only for $z \leq 1$ and is not present at higher redshifts where the patterns are similar to the F5 and F6 models. We can also discern a dip developing with time at scales ∼45–$50\,h^{-1}$ Mpc, with the scale of the dip being smaller for higher order amplitude. The dip is weakly visible for the ΔS_3, albeit it gets much stronger and clearer for the kurtosis and especially the S_5 case. The scale of this feature coincides strongly with the scale of the first dip from the BAO wiggle observed in hierarchical amplitudes of the fiducial GR model by Hellwing et al. (2013, see fig. 1). Thus, we speculate that due to the extended non-linear evolution observed in the F4 model, the BAO signal naturally present at this scales in hierarchical amplitudes (Juszkiewicz et al. 2013) gets enhanced in our strongest $f(R)$ model. This behaviour can have potentially observable consequences as the BAO signal will be measured with a per cent-level accuracy in forthcoming galaxy redshift surveys. Unfortunately, the detailed analysis of this phenomena lies beyond the scope of this paper and we leave it for the future work.

Finally, we note the complicated pattern of the deviations in time evolution seen at small scales ($R_{TH} < 10\,h^{-1}$ Mpc). In contrast with the F5 and F6 models, at those scales the relative deviations keep growing steadily also at late times $z \leq 0.6$. Moreover. we observe that for a few redshifts and scales, the monotonic time dependence of the growth of the relative deviations is broken. This is clearly visible for ΔS_4 and ΔS_5, as we can find snapshots where the values

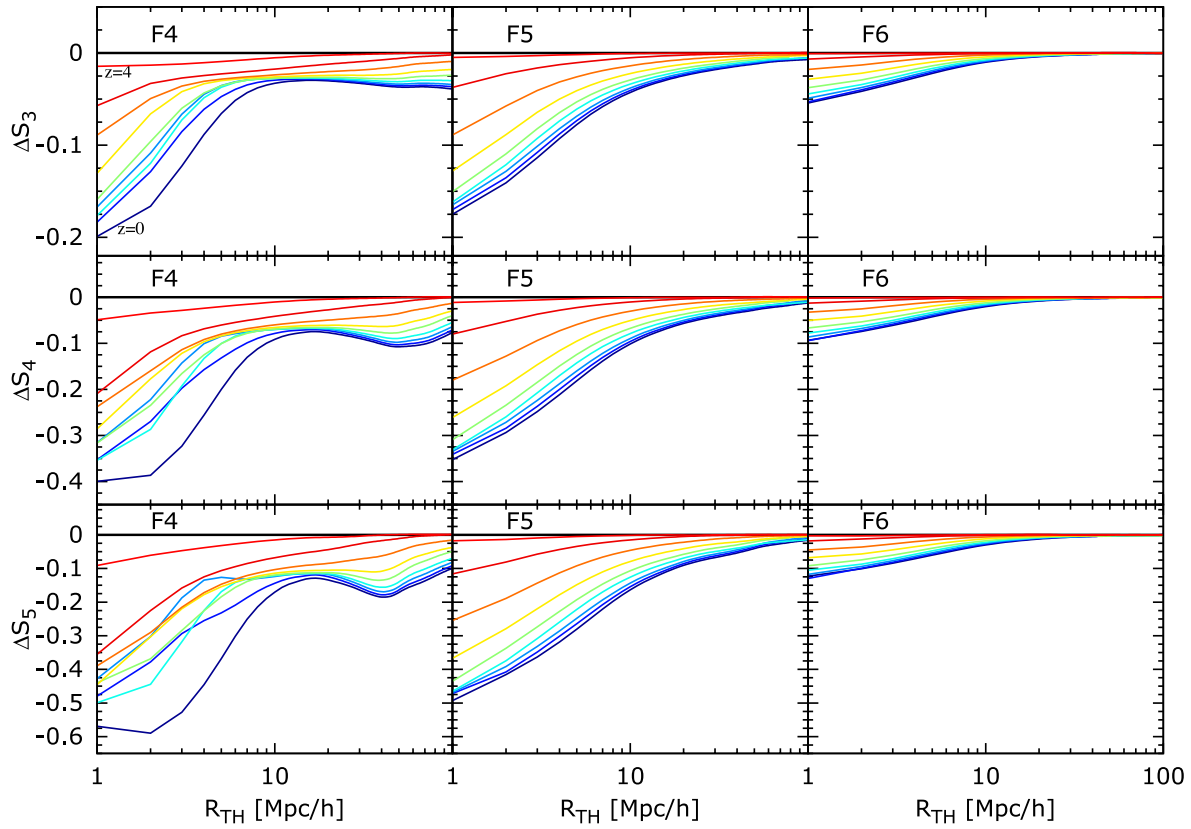

Figure 10. Time evolution of the skewness (top-row panels), the kurtosis (middle-row panels) and S_5 (bottom-most panels) deficiency with respect to the fiducial GR model. The leftmost columns show the F4 model, the centre columns marks the F5, while the rightmost panels corresponds to the F6 flavour. The data are from $1000\,h^{-1}$ Mpc ensemble.

at $R \sim 5\,h^{-1}$ Mpc are actually higher for early times (e.g. $z = 0.6$) rather than for later (e.g. $z = 0.25$). We assign this complicated and unexpected, at first sight, behaviour of the density field distribution functions with the low efficiency of the chameleon mechanism in the F4 model. Due to this, the fifth-force in this model is largely unscreened for all scales of interest. This induces much higher order of non-linearity of the density field in the F4 model (as already indicated by much higher variance) and makes the transfer of the power from small to large scales more efficient. As this non-linear tenue is strongly enhanced for the F4 model, this is not observed for the F5 and F6 $f(R)$ models, where the chameleon and scalaron mechanism are subject to a more graceful evolution.

5.5 Density distribution functions

In the previous paragraphs, we have assessed the patterns of the $f(R)$ gravity visible in the hierarchical amplitudes and their time evolution as the relative deviations from the values predicted for the standard gravity limit. As discussed before for a Gaussian random field all cumulants of the density field probability distribution function (PDF) except for the variance vanish. The non-zero higher order cumulants of the PDF measure the shape deviations of the distribution function from a Gaussian. Thus, in this section, we look directly at the PDFs computed for all our models for fields smoothed with six different top-hat radii. For completeness, we recall the definition

$$\mathrm{PDF}(\eta) = \frac{P(\eta)}{\mathrm{d}\eta} \cong \frac{P(\eta)}{\Delta\eta}\,, \tag{30}$$

where $\eta \equiv \delta + 1$ and the probability $P(\eta)$ is measured in practice as a frequency probability using

$$P(\eta) = \frac{1}{N_\mathrm{g}} \sum_{i=0}^{N_\mathrm{g}} (\eta_i : \eta < \eta_i \leq \eta + \Delta\eta)\,. \tag{31}$$

Here, the N_g is the number of the grid points sampling the smoothed density field and we choose to keep the bin width $\Delta\eta$ constant in the logarithmic space.

In Fig. 11, we present the PDFs computed for the $1000\,h^{-1}$ Mpc box simulations, where in each panel the black solid line marks the GR value, while the red, blue and green solid lines correspond to the F4, F5 and F6 models. We start from the $R_\mathrm{TH} = 2\,h^{-1}$ Mpc for the top-left panel and increase the window size from left to right and from top to bottom, ending with $R_\mathrm{TH} = 34\,h^{-1}$ Mpc shown in the bottom-right panel. The general trends abide the $f(R)$ PDFs that are shifted towards lower density contrast values when compared with the GR. This shift is accompanied only by a very small excess in the positive tail of the density distribution. This excess is barely visible in our plot as we choose to use linear rather than logarithmic scale on our x-axis. Commonly adopted convention is to plot PDF in the logarithmic space. We drop the logarithmic scaling on the PDF values since it over-represents rare events (cells with very high $\delta + 1$ values). By construction, our DTFE-estimated density field is volume weighted (recall the Section 3.1), and as the volume of the Universe is dominated by cosmic voids (Bond, Kofman & Pogosyan 1996; Aragón-Calvo et al. 2010; Shandarin, Habib & Heitmann 2012; Cautun, van de Weygaert & Jones 2013), it is clear that the modified gravity signal we see in the dislocated shape of the PDFs is coming

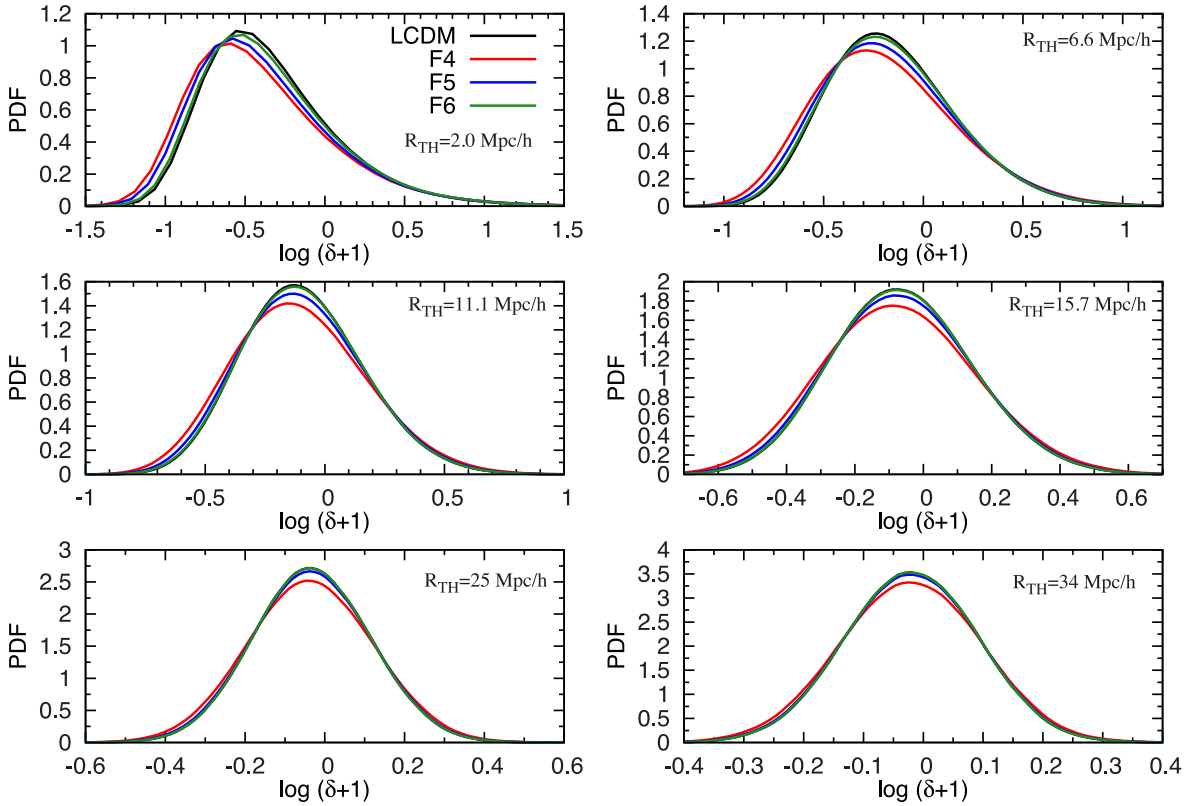

Figure 11. The probability distribution functions (PDFs) for the density field $\delta + 1$ computed using various top-hat windows. For each panel, we plot PDFs for our four models marked by solid colour lines as: GR (black), F4 (red), F5 (blue) and F6 (green). From top to down and left to right, the panels illustrate the distribution functions of a field smoothed at larger and larger scales, starting from $R_{\rm TH} = 2\,h^{-1}$ Mpc for the top-left panel and ending at $R_{\rm TH} = 34\,h^{-1}$ Mpc for the bottom-right one. See the text for more details.

mostly from the cosmic voids. The last statement also holds for the patterns we saw in the reduced skewness, kurtosis and S_5. The departure of $f(R)$ distribution functions from the GR case is quickly decreasing with the increasing radius of the smoothing top-hat, in agreement with the behaviour observed earlier for the hierarchical amplitudes. At scales $R_{\rm TH} \sim 25{-}34\,h^{-1}$ Mpc, the F5, F6 and GR PDFs become indistinguishable. The strongest F4 model still bears some signal, although it is mostly contained in a modified PDF amplitude at the mean-field values (around $\delta \sim 0$) rather than the PDF shape. The deeper voids (less dense) are characteristic mark for the modified gravity models employing the scalar fifth-force. This was established by many authors (Hellwing & Juszkiewicz 2009; Li 2011; Li, Zhao & Koyama 2012b; Clampitt, Cai & Li 2013). As we do not employ any void-finding algorithms in our studies, we probe the void population indirectly, only in statistical sense, by measuring the density field PDFs for various radii. Still we can confirm that, when one is concerned with the density field clustering statistics, it is the cosmic voids that are the most sensitive parts of the cosmic web, provided that one is interested in the modified gravity effects. This is especially true for the chameleon class of $f(R)$ gravity models that we study here. This is due to the fact, that the low density in voids prevents the chameleon mechanism from screening out the fifth-force of the scalaron at later stages of evolution (Li 2011; Clampitt et al. 2013). Hence, the fifth-force in deep voids is allowed to quickly saturate to its maximum enhancement value of $1/3$.

The $f(R)$ gravity effects seen in the PDFs from Fig. 11 indicate that in statistical sense we have many more parts of the density field where the density contrast is lower than in the GR case. Since our simulations share the same initial phases the density fields both in $f(R)$ and GR share the same number of initial peaks (haloes) and dips (voids). At small scales, the non-linear evolution can significantly alter the number of peaks and dips due to halo and void mergers as well as the *void-in-cloud* process (void squashing; see Sheth & van de Weygaert 2004; Paranjape, Lam & Sheth 2012; Jennings, Li & Hu 2013). However, at larger scales beyond the cluster sizes $R_{\rm TH} \gtrsim 5\,h^{-1}$ Mpc this non-linear processes are much less important and do not affect much the initial peak/dip counts (Bardeen et al. 1986). Therefore, starting from the smoothing radius $R_{\rm TH} = 6.6\,h^{-1}$ Mpc (the top-right panel in the figure) the density fields of the GR and $f(R)$ simulations should have roughly closely matching count statistics of the number of peaks and dips. If this hypothesis is true, the PDF shifts observed in Fig. 11 would indicate that in $f(R)$ gravity we deal with cosmic voids that are emptier than their GR cousins. Since during the evolution of the Universe the continuity equations holds everywhere (conservation of mass), the enhanced emptying of the voids must be followed by an increased mass of the cluster and galaxy haloes. This was already observed (Schmidt et al. 2009a; Li et al. 2012b).

We can now understand why the $f(R)$ gravity clustering hierarchy has PDFs characterized by lower values of the reduced cumulants than the GR case. Let us consider the gravitational instability mechanism that governs the shape evolution of the density distribution function. As the voids get more empty, the matter flow via walls and filaments towards dense nodes of the cosmic web – the galaxy clusters (Bond et al. 1996). This process naturally lowers the density contrast in voids, while raising it in the more dense clusters and

filaments. The lower density $\delta < 0$ tail of the distribution function is constrained from the left-hand side by a natural physical limit of $\delta > -1$. The density contrast cannot be lower than this, since $\delta = -1$ already indicates empty space. At the same time, the right-hand tail of the PDF can grow towards arbitrarily high-δ values as the matter accretion, halo mergers and violent relaxation proceed. This asymmetry, intrinsically connected with the gravitational instability mechanism, implies growth with time of the skewness, kurtosis and higher order cumulants. The enhanced clustering exhibited by the $f(R)$ models provides much empty voids and this process dominates over the mass increase of clusters (due to the volume dominance of the voids). The overall effect shifts the PDF towards the lower density tail.

6 CONCLUDING REMARKS

Having assessed all parts of the DM hierarchical clustering in chameleon $f(R)$ gravity we can conduct the summary of our results. We begin by noting that both fiducial GR (LCDM) model and our three flavours of $f(R)$ models start from the same initial conditions, currently tightly constrained by high-redshift Universe observations like the cosmic background radiation temperature and polarization anisotropy maps (Hinshaw et al. 2012; Planck Collaboration 2013). The starting point for all our models is the primordial post-inflationary density perturbation field that has Gaussian statistics. The primordial field is then propagated using the Zel'Dovich approximation down to the initial redshift of $z_i = 49$. The transients induced by this procedure are relaxed by the real dynamics followed by the N-body simulations. In addition, the background cosmology as well as the expansion history is shared among all models down to $z = 0$. Albeit the growth history of the $f(R)$ models traces the GR values only for $z \gtrsim 5$, for the remaining part of the cosmic evolution the fifth-force starts to modify the matter dynamics. Thus, all departures of the clustering statistics present in the $f(R)$ universes must be accounted for by the late-time altered dynamics induced by the modified gravity of those models.

The effects of the scalar force dynamics are not trivial to predict, especially at later evolutionary stages. This is due to the presence of the chameleon mechanism and its non-linear nature reciprocally connected with high-density peaks (haloes). The highly non-linear nature associated with the chameleon screening quickly renders all PT results inaccurate in their description of the clustering statistics for the class of $f(R)$ models studied here (e.g. Li & Zhao 2009; Li et al. 2012b, 2013). Our employment of the series of high-resolution, state-of-the-art N-body simulations of the chameleon $f(R)$ gravity allowed us to perform a robust and consistent analysis.

Using our simulations, we have constructed high-resolution volume-weighed DTFE density fields and have used these to compute the high-order correlation functions and hierarchical amplitudes up to, respectively, ninth and eighth order. We have also traced the time evolution of the reduced cumulants focusing on the skewness, kurtosis and S_5 amplitudes and the redshift evolution of the relative deviation of these quantities from the fiducial GR case. Finally, we have computed the density PDFs for a set of the smoothing scales. We can summarize our findings in the following points.

(i) The $f(R)$ density fields are characterized by higher variance σ^2. The deviation from the GR case is strongest at the smallest scales reliably probed by our simulations $R \sim 2{-}3\,h^{-1}$ Mpc and can reach nearly $\sim$50 per cent of enhancement for F4 model. The effect is weaker for F5 ($\sim$20 per cent maximal enhancement) and marginal for F6. The excess of the variance quickly drops with the smoothing scale. However, for the F4, it is still of the order of 5 per cent at $100\,h^{-1}$ Mpc.

(ii) Increased variance of the DM density induces higher σ_8 values for the modified gravity. We can report that the non-linear σ_8 is higher by 14 per cent in F4, 5 per cent in F5 and 0.7 per cent in F6 models, and this excess from the GR is statistically significant.

(iii) All measured volume-averaged correlation functions $\overline{\xi}_n$, up to ninth order have higher values for chameleon gravity at small, non-linear scales. However, above $R > \sim 30\,h^{-1}$ Mpc for all our $f(R)$ models, the correlation functions start to converge to the GR values within 1σ cosmic variance scatter.

(iv) We have found that the hierarchical scaling is also present in the $f(R)$ gravity. The modified dynamics induced by the fifth-force changes however the values of the hierarchical amplitudes S_n and their scale dependence w.r.t. the standard gravitational instability predictions. The values of the modified gravity scaling amplitudes are always lower than in the GR case. In the case of the F4 and F5 models, the lower values of the skewness, kurtosis and S_5 appear for all smoothing scales probed by us, up to $100\,h^{-1}$ Mpc.

(v) We have measured an interesting behaviour of the relative deviations for $\Delta S_{3,4,5}$ at scales $R \lesssim 10\,h^{-1}$ Mpc for the F5 and F4 models. At those scales, the F5 model shows higher deviations from the LCDM case than the F4 model. We attribute this behaviour to the non-linear evolution of the density field and the screening effect of the chameleon, which is present in the F5 and barely active in F4. Also for all models, the relative deviations grow with the increasing order of the S_n.

(vi) The evolution of the $\Delta S_{3,4,5}$ is monotonic in time. For $z > 5$, the departures from the standard model are negligible and start to grow quickly for later times. All models exhibit the fastest growth at moderate redshifts $1 \leq z \leq 4$. At late evolutionary stages, the departures from the GR experience much steadier growth. This picture however becomes much more complicated for the strongest F4 model. Here, we have observed a highly non-linear pattern of scale and time dependence of the relative deviation parameters $\Delta S_{3,4,5}$. We believe that this effect is due to severely enhanced non-linearities in the density field present in the F4 universe.

(vii) The PDFs of the $f(R)$ density fields are significantly shifted towards the $\delta \to -1$ tail. This can be observed for scales up to $R_{\rm TH} \sim 20\,h^{-1}$ Mpc. Hence, in a statistical sense, the $f(R)$ gravity produces much emptier and deeper cosmic voids.

Our findings summarized above paint a picture in which the $f(R)$ gravitational instability and dynamics induce significant differences in the degree of the DM density field correlations at small scales. The most important message is that the hierarchical scaling is preserved in this class of models as well. Albeit we can denote that at scales relevant to the galaxy and halo formation, the $f(R)$ density field is characterized by enhanced clustering at all correlation orders.

Before any comparison of our theoretical predictions to observations can be made, we need to briefly address three possible sources of confusion.

(i) *Galaxy biasing*. If the galaxy formation process varies in efficiency with environment, then the galaxy distribution may foster a biased picture of the underlying mass distribution. If we assume that the smoothed galaxy density field $\delta_{\rm g}$ is a local, but not necessarily a linear function of the smoothed DM density field: $\delta_{\rm g}(x) = F[\delta(x)]$, where F is an arbitrary function, then by using a Taylor expansion of F for $|\delta| \ll 1$, it can be shown, as Fry & Gaztanaga (1993) did, that local biasing preserves the form of the scaling relations (16). As the scaling relations for the galaxy density field are preserved, the values of the hierarchical amplitudes S_n are necessarily not. If we

consider for example the reduced skewness S_3, the galaxy biasing will change it to (Fry & Gaztanaga 1993)

$$S_{3g} \equiv \langle\delta_g^3\rangle/\langle\delta_g^2\rangle = b_1^{-1}S_3 + 3b_2/b_1^2\,, \quad (32)$$

where $b_n \equiv \mathrm{d}^nF/\mathrm{d}\delta^n$, evaluated at $\delta = 0$. The bias parameters can be also scale dependent (and in realistic models they indeed are). Generally, the $f(R)$ model will differ from the GR by the values of the b_n parameters. In the worst case scenario, all clustering effects induced by the chameleon $f(R)$ gravity may be camouflaged as the scale-dependent relative bias differences $b_n^{f(R)}/b_n^{GR}$, and indeed this was already shown to some extent by Schmidt et al. (2009a). Unfortunately, both the GR and $f(R)$ gravity can then predict the same values of $\langle\delta_g^n\rangle_c$ and S_{ng}. Hence, the modified gravity signal will be visible only in a difference in the scale dependence of the bias parameters to that in the GR. The detailed discussion of this situation is beyond the scope of this work. We will analyse it in the forthcoming paper (Hellwing et al., in preparation).

(ii) *Redshift space distortions*. This is yet another important difficulty which needs to be considered before the theoretical predictions can be meaningfully compared with the data from galaxy redshift surveys. In such catalogues, radial velocities of galaxies are used instead of their true radial coordinates. As a result, peculiar motions of galaxies distort their true spatial distribution and the n-point correlation functions (e.g. Fry & Gaztanaga 1994). Both Bouchet et al. (1995) and Hivon et al. (1995), using the Lagrangian PT and N-body simulations, studied the effects of the redshift distortions on ξ_2, ξ_3 and S_3. They showed that albeit both ξ_2 and ξ_3 are affected by the redshift space distortion, all appreciable effects cancel out for the reduced skewness S_3. Thus, the comparison between theoretical predictions and observations should not be obscured by the redshift space provided we use the moment ratio S_3 rather than the correlation functions themselves. However, this was only shown to be true for the standard gravitational instability mechanism acting within the GR framework. The picture could be changed in $f(R)$ gravity. Here, the peculiar velocity power spectra have higher amplitudes at small and moderate scales as shown by Li et al. (2013). This inevitably leads to a modified amplitude of the redshift space distortions as shown by Jennings et al. (2012) for the 2-point statistics. Whether or not this will strongly change the sensitivity to the redshift distortions of the moments ratios S_n is not known. This problem must be studied before any galaxy-clustering data can be used to constrain $f(R)$ models.

(iii) *The effect of baryons*. All our simulations discussed here contain only the DM. The only baryonic effects we included in the simulations were encoded in the initial transfer functions (the BAO wiggles) and increased DM density parameter which was set to be equal to the sum of Ω_{DM} and Ω_b. In other words, baryons in our simulations were treated as DM. However, it is well known that baryon content of the Universe is a subject of a complicated and intrinsically non-linear hydrodynamical evolution, including effects such as radiative cooling, reionization, supernova and AGN feedbacks. It is well established that in the presence of those effects the higher order clustering hierarchy can be significantly altered at small scales (e.g. Guillet et al. 2010). The modified non-linear dynamics of the $f(R)$ gravity models can only add to the overall complicated picture associated with the baryon content. Recently, Puchwein, Baldi & Springel (2013) have used an $f(R)$-enabled version of the GADGET2 (Springel 2005) to show that at small scales the effects induced by the $f(R)$ gravity in the matter power spectrum have the opposite sign to the effects coming from baryonic physics (i.e. supernova and AGN feedbacks). The baryonic effects studied by Puchwein et al. (2013) appear on similar scales and have comparable magnitudes to the effects of the modified $f(R)$ gravity. This shows that there are considerable degeneracies between the modified gravity and baryonic effects, provided that one is concerned with the power spectrum only.

The general picture emerging from our studies is the following. The $f(R)$ gravity introduces significant modifications in the higher order clustering statistics that are especially strong at small scales, unfortunately the complicated nature of the galaxy formation process will make it very difficult to rule out or constrain this class of models using data on spatial clustering of galaxies alone.

ACKNOWLEDGEMENTS

We would like to thank anonymous referee of this paper for helping us improve the quality of the manuscript. The simulations and their analysis presented in this paper were carried out using the *cosmology machine* at the University of Durham. We would like to acknowledge Lydia Heck whose technical support made our computations much more smooth. WAH acknowledge the support received from Polish National Science Center in grant no. DEC-2011/01/D/ST9/01960 and ERC Advanced Investigator grant of C. S. Frenk, COSMIWAY. BL is supported by the Royal Astronomical Society and Durham University. The N-body simulations presented in this paper were run on the ICC Cosmology Machine, which is part of the DiRAC Facility jointly funded by STFC, the Large Facilities Capital Fund of BIS and Durham University.

REFERENCES

Amendola L., 2000, Phys. Rev. D, 62, 043511
Angulo R. E., Baugh C. M., Lacey C. G., 2008, MNRAS, 387, 921
Aragón-Calvo M. A., Platen E., van de Weygaert R., Szalay A. S., 2010, ApJ, 723, 364
Bardeen J. M., Bond J. R., Kaiser N., Szalay A. S., 1986, ApJ, 304, 15
Baugh C. M., Gaztanaga E., Efstathiou G., 1995, MNRAS, 274, 1049
Baugh C. M. et al., 2004, MNRAS, 351, L44
Bean R., Bernat D., Pogosian L., Silvestri A., Trodden M., 2007, Phys. Rev. D, 75, 064020
Bernardeau F., 1992, ApJ, 392, 1
Bernardeau F., 1994, A&A, 291, 697
Bernardeau F., 2004, arXiv:e-prints
Bernardeau F., Colombi S., Gaztañaga E., Scoccimarro R., 2002, Phys. Rep., 367, 1
Berry C. P. L., Gair J. R., 2011, Phys. Rev. D, 83, 104022
Bond J. R., Kofman L., Pogosyan D., 1996, Nat, 380, 603
Borisov A., Jain B., 2009, Phys. Rev. D, 79, 103506
Bouchet F. R., Hernquist L., 1992, ApJ, 400, 25
Bouchet F. R., Colombi S., Hivon E., Juszkiewicz R., 1995, A&A, 296, 575
Brax P., van de Bruck C., Davis A.-C., Shaw D. J., 2008, Phys. Rev. D, 78, 104021
Brax P., van de Bruck C., Davis A.-C., Li B., Shaw D. J., 2011, Phys. Rev. D, 83, 104026
Brax P., Davis A.-C., Li B., Winther H. A., 2012, Phys. Rev. D, 86, 044015
Brookfield A. W., van de Bruck C., Hall L. M. H., 2006, Phys. Rev. D, 74, 064028
Carroll S. M., 2001, Living Rev. Relativ., 4, 1
Carroll S. M., Duvvuri V., Trodden M., Turner M. S., 2004, Phys. Rev. D, 70, 043528
Carroll S. M., De Felice A., Duvvuri V., Easson D. A., Trodden M., Turner M. S., 2005, Phys. Rev. D, 71, 063513
Cautun M. C., van de Weygaert R., 2011, arXiv:e-prints
Cautun M., van de Weygaert R., Jones B. J. T., 2013, MNRAS, 429, 1286
Chiba T., 2003, Phys. Lett. B, 575, 1
Chiba T., Smith T. L., Erickcek A. L., 2007, Phys. Rev. D, 75, 124014

Clampitt J., Cai Y.-C., Li B., 2013, MNRAS, 431, 749
Cole S. et al., 2005, MNRAS, 362, 505
Colombi S., Bouchet F. R., Schaeffer R., 1994, A&A, 281, 301
Crocce M., Pueblas S., Scoccimarro R., 2006, MNRAS, 373, 369
Croton D. J. et al., 2004, MNRAS, 352, 1232
Davis A.-C., Li B., Mota D. F., Winther H. A., 2012, ApJ, 748, 61
de Felice A., Tsujikawa S., 2010, Living Rev. Relativ., 13, 3
Eisenstein D. J. et al., 2005, ApJ, 633, 560
Erickcek A. L., Barnaby N., Burrage C., Huang Z., 2013, Phys. Rev. Lett., 110, 171101
Faulkner T., Tegmark M., Bunn E. F., Mao Y., 2007, Phys. Rev. D, 76, 063505
Feldman H. et al., 2003, ApJ, 596, L131
Fry J. N., 1984a, ApJ, 277, L5
Fry J. N., 1984b, ApJ, 279, 499
Fry J. N., Gaztanaga E., 1993, ApJ, 413, 447
Fry J. N., Gaztanaga E., 1994, ApJ, 425, 1
Gaztanaga E., 1994, MNRAS, 268, 913
Gaztanaga E., Baugh C. M., 1995, MNRAS, 273, L1
Gaztanaga E., Bernardeau F., 1998, A&A, 331, 829
Gaztañaga E., Norberg P., Baugh C. M., Croton D. J., 2005, MNRAS, 364, 620
Goroff M. H., Grinstein B., Rey S.-J., Wise M. B., 1986, ApJ, 311, 6
Guillet T., Teyssier R., Colombi S., 2010, MNRAS, 405, 525
Hellwing W. A., Juszkiewicz R., 2009, Phys. Rev. D, 80, 083522
Hellwing W. A., Juszkiewicz R., van de Weygaert R., 2010, Phys. Rev. D, 82, 103536
Hellwing W. A., Juszkiewicz R., van de Weygaert R., Bilicki M., 2013, arXiv:e-prints
Hinshaw G. et al., 2012, arXiv:e-prints
Hivon E., Bouchet F. R., Colombi S., Juszkiewicz R., 1995, A&A, 298, 643
Hu W., Sawicki I., 2007, Phys. Rev. D, 76, 064004
Jennings E., Baugh C. M., Li B., Zhao G.-B., Koyama K., 2012, MNRAS, 425, 2128
Jennings E., Li Y., Hu W., 2013, MNRAS, 434, 2167
Juszkiewicz R., Bouchet F. R., 1995, in Maurogordato S., Balkowski C., Tao C., Tran Thanh Van J., eds, Proc. 30th Rencontres de Moriond, Clustering in the Universe. Editions Frontiers, Paris, p. 167
Juszkiewicz R., Bouchet F. R., Colombi S., 1993, ApJ, 412, L9
Juszkiewicz R., Feldman H. A., Fry J. N., Jaffe A. H., 2010, J. Cosmol. Astropart. Phys., 2, 21
Juszkiewicz R., Hellwing W. A., van de Weygaert R., 2013, MNRAS, 429, 1206
Kamenshchik A., Moschella U., Pasquier V., 2001, Phys. Lett. B, 511, 265
Kendall M., Stuart A., 1977, The Advanced Theory of Statistics. Vol. 1: Distribution Theory, Griffin, London
Khoury J., Weltman A., 2004, Phys. Rev. D, 69, 044026
Koivisto T., 2006, Phys. Rev. D, 73, 083517
Łokas E. L., Juszkiewicz R., Weinberg D. H., Bouchet F. R., 1995, MNRAS, 274, 730
Li B., 2011, MNRAS, 411, 2615
Li B., Barrow J. D., 2007, Phys. Rev. D, 75, 084010
Li B., Barrow J. D., 2011, Phys. Rev. D, 83, 024007
Li B., Zhao H., 2009, Phys. Rev. D, 80, 044027
Li B., Zhao H., 2010, Phys. Rev. D, 81, 104047
Li B., Zhao G.-B., Teyssier R., Koyama K., 2012a, J. Cosmol. Astropart. Phys., 1, 51
Li B., Zhao G.-B., Koyama K., 2012b, MNRAS, 421, 3481
Li B., Hellwing W. A., Koyama K., Zhao G.-B., Jennings E., Baugh C. M., 2013, MNRAS, 428, 743
Mota D. F., Shaw D. J., 2007, Phys. Rev. D, 75, 063501
Navarro I., Van Acoleyen K., 2007, J. Cosmol. Astropart. Phys., 2, 22
Nojiri S., Odintsov S. D., 2011, Phys. Rep., 505, 59
Oyaizu H., 2008, Phys. Rev. D, 78, 123523
Oyaizu H., Lima M., Hu W., 2008, Phys. Rev. D, 78, 123524
Paranjape A., Lam T. Y., Sheth R. K., 2012, MNRAS, 420, 1648
Peebles P. J. E., 1980, The Large-Scale Structure of the Universe. Princeton Univ. Press, Princeton, NJ, p. 435
Peebles P. J. E., Ratra B., 1988, ApJ, 325, L17
Perlmutter S. et al., 1999, ApJ, 517, 565
Planck Collaboration, 2013, arXiv:e-prints
Puchwein E., Baldi M., Springel V., 2013, arXiv:e-prints
Ratra B., Peebles P. J. E., 1988, Phys. Rev. D, 37, 3406
Riess A. G. et al., 1998, AJ, 116, 1009
Ross A. J., Brunner R. J., Myers A. D., 2007, ApJ, 665, 67
Schaap W. E., van de Weygaert R., 2000, A&A, 363, L29
Schmidt F., 2009, Phys. Rev. D, 80, 043001
Schmidt F., Lima M., Oyaizu H., Hu W., 2009a, Phys. Rev. D, 79, 083518
Schmidt F., Vikhlinin A., Hu W., 2009b, Phys. Rev. D, 80, 083505
Scoccimarro R., 1998, MNRAS, 299, 1097
Shandarin S., Habib S., Heitmann K., 2012, Phys. Rev. D, 85, 083005
Sheth R. K., van de Weygaert R., 2004, MNRAS, 350, 517
Song Y.-S., Hu W., Sawicki I., 2007, Phys. Rev. D, 75, 044004
Sotiriou T. P., Faraoni V., 2010, Rev. Mod. Phys., 82, 451
Springel V., 2005, MNRAS, 364, 1105
Szapudi I., Colombi S., 1996, ApJ, 470, 131
Szapudi I., Quinn T., Stadel J., Lake G., 1999, ApJ, 517, 54
Tatekawa T., Mizuno S., 2007, J. Cosmol. Astropart. Phys., 12, 14
Tatekawa T., Tsujikawa S., 2008, J. Cosmol. Astropart. Phys., 9, 9
Tegmark M. et al., 2004, ApJ, 606, 702
Teyssier R., 2002, A&A, 385, 337
van de Weygaert R., Schaap W., 2009, in Martínez V. J., Saar E., Martínez-González E., Pons-Bordería M.-J., eds, Lecture Notes in Physics, Vol. 665, Data Analysis in Cosmology. Springer, Berlin, p. 291
Watkins R., Feldman H. A., Hudson M. J., 2009, MNRAS, 392, 743
Zaldarriaga M., Seljak U., Hui L., 2001, ApJ, 551, 48
Zel'Dovich Y. B., 1970, A&A, 5, 84
Zhao G.-B., Li B., Koyama K., 2011, Phys. Rev. D, 83, 044007
Zlatev I., Wang L., Steinhardt P. J., 1999, Phys. Rev. Lett., 82, 896

This paper has been typeset from a TEX/LATEX file prepared by the author.